

**A COMPARATIVE STUDY OF FIVE  
ALGORITHMS FOR PROCESSING  
ULTRASONIC ARC MAPS**

A THESIS

SUBMITTED TO THE DEPARTMENT OF ELECTRICAL AND  
ELECTRONICS ENGINEERING

AND THE INSTITUTE OF ENGINEERING AND SCIENCE  
OF BILKENT UNIVERSITY

IN PARTIAL FULFILLMENT OF THE REQUIREMENTS

FOR THE DEGREE OF  
MASTER OF SCIENCE

By

Arda Kurt

August 2005

I certify that I have read this thesis and that in my opinion it is fully adequate, in scope and in quality, as a thesis for the degree of Master of Science.

---

Prof. Dr. Billur Barshan(Supervisor)

I certify that I have read this thesis and that in my opinion it is fully adequate, in scope and in quality, as a thesis for the degree of Master of Science.

---

Assoc. Prof. Dr. Orhan Arıkan

I certify that I have read this thesis and that in my opinion it is fully adequate, in scope and in quality, as a thesis for the degree of Master of Science.

---

Asst. Prof. Dr. H. Murat Karamüftüođlu

Approved for the Institute of Engineering and Science:

---

Prof. Dr. Mehmet Baray  
Director of the Institute Engineering and Science

## ABSTRACT

# A COMPARATIVE STUDY OF FIVE ALGORITHMS FOR PROCESSING ULTRASONIC ARC MAPS

Arda Kurt

M.S. in Electrical and Electronics Engineering

Supervisor: Prof. Dr. Billur Barshan

August 2005

In this work, one newly proposed and four existing algorithms for processing ultrasonic arc maps are compared for map-building purposes. These algorithms are the directional maximum, Bayesian update, morphological processing, voting and thresholding, and arc-transversal median algorithm. The newly proposed method (directional maximum) has a basic consideration of the general direction of the mapped surface. Through the processing of arc maps, each method aims at overcoming the intrinsic angular uncertainty of ultrasonic sensors in map building, as well as eliminating noise and cross-talk related misreadings. The algorithms are implemented in computer simulations with two distinct motion-planning schemes for ground coverage, wall following and Voronoi diagram tracing. As success criteria of the methods, mean absolute difference with the actual map/profile, fill ratio, and computational cost in terms of CPU time are utilized. The directional maximum method performed superior to the existing algorithms in mean absolute error, was satisfactory in fill ratio and performed second best in processing times. The results indicate various trade-offs in the choice of algorithms for arc-map processing.

*Keywords:* Ultrasonic sensors, map building, arc maps, Bayesian update scheme, morphological processing, voting and thresholding, arc-transversal median algorithm, wall following, Voronoi diagram, motion planning, mobile robots.

## ÖZET

# ULTRASONİK ARK HARİTASI İŞLEMENE DAYALI BEŞ YÖNTEMİN KARŞILAŞTIRMALI İNCELEMESİ

Arda Kurt

Elektrik Elektronik Mühendisliği, Yüksek Lisans

Tez Yöneticisi: Prof. Dr. Billur Barshan

Ağustos 2005

Bu çalışmada, biri yeni geliştirilmiş, dördü ise önceden varolan, ultrasonik ark haritası işleyerek harita çıkarımına yönelik beş yöntem karşılaştırılmıştır. Bu yöntemler sırasıyla yönlü maksimum, Bayesian güncelleme, morfolojik işleme, oylama ve eşikleme, ve ark-doğrultusal medyan yöntemleridir. Yeni geliştirilen yöntem (yönlü maksimum), haritalanan yüzeyin genel doğrultusuna dair temel bir bilgiyi işleme dahil etmektedir. Tüm yöntemler ark haritaları işleme yoluyla ultrasonik algılayıcılara özgü açısız belirsizliğin, sinyal gürültüsünün ve çapraz-konuşmanın haritalamaya olumsuz etkilerini ortadan kaldırmayı hedeflemektedir. Karşılaştırma amaçlı bilgisayar benzetimlerinde alan kapsamaya yönelik olarak duvar takibi ve Voronoi grafiği çizimi taramaya dayalı iki değişik hareket-planlama yöntemi kullanılmıştır. Başarım ölçütü olarak çıkarılan haritanın gerçek profil ile arasındaki ortalama mutlak fark, gerçek haritanın ne oranda çıkarılabildiğine dair doluluk oranı ve işlemin bilgisayar ortamında aldığı süre kullanılmıştır. Yeni öne sürülen yöntem olan yönlü maksimum ortalama mutlak hata alanında diğer yöntemlerden daha yüksek bir başarı sergilemiş, doluluk oranında başarılı olmuş, hesaplama süresinde de ikinci en iyi dereceyi elde etmiştir. Yöntem seçiminde her yöntemin kendine özgü avantaj ve dezavantajları göz önünde bulundurulmalıdır.

*Anahtar sözcükler:* Ultrasonik algılayıcılar, haritalama, ark haritaları, Bayesian güncelleme, morfolojik işleme, oylama ve eşikleme, ark-doğrultusal medyan yöntemi, duvar takibi, Voronoi grafiği çizimi, hareket planlama, gezer robotlar.

# Contents

<b>1</b>	<b>Introduction</b>	<b>1</b>
<b>2</b>	<b>Basics of Ultrasonic Sensing</b>	<b>4</b>
2.1	Ultrasonic Transducers . . . . .	4
2.2	Ultrasonic Time-of-Flight Measurement . . . . .	6
2.3	Representing Angular Uncertainty by Arc Maps . . . . .	9
<b>3</b>	<b>Algorithm Descriptions</b>	<b>11</b>
3.1	Bayesian Update (BU) . . . . .	11
3.2	Morphological Processing (MP) . . . . .	17
3.3	Voting and Thresholding (VT) . . . . .	19
3.4	Arc-Transversal Median (ATM) . . . . .	20
3.5	Directional Maximum (DM) . . . . .	21
3.6	Results of Simulation Examples . . . . .	23
<b>4</b>	<b>Indoor Mapping Simulations</b>	<b>25</b>

4.1	Wall Following (WF) . . . . .	25
4.2	Voronoi Diagram (VD) Tracing . . . . .	35
4.3	Results of Indoor Mapping Simulations . . . . .	44
<b>5</b>	<b>Conclusions</b>	<b>48</b>
<b>A</b>	<b>Ultrasonic Signal Models</b>	<b>50</b>
<b>B</b>	<b>Wall-following (WF) Algorithm</b>	<b>52</b>
<b>C</b>	<b>MATLAB Simulation Codes</b>	<b>55</b>

# List of Figures

2.1	Typical received echo with additive noise and the threshold level. . .	7
2.2	(a) Single transducer configuration resulting in a <i>circular</i> arc, (b) dual transceiver configuration resulting in an <i>elliptical</i> arc. . . . .	8
3.1	(a) Range dependency, (b) $x$ and $y$ dependency, and (c) $\theta$ dependency of $p_O$ and $p_E$ . . . . .	13
3.2	Simulation example 1 – actual surface profile and the transducer positions. . . . .	14
3.3	Simulation example 2 – actual object and the transducer positions. . .	14
3.4	Arc maps of the two simulation examples. . . . .	16
3.5	Example 1 – BU result for occupancy probabilities. . . . .	17
3.6	Example 1 – MP results (opening applied). . . . .	18
3.7	Example 2 – VT with a threshold of 5. . . . .	19
3.8	Example 2 – ATM. . . . .	20
3.9	DM results on the two examples. . . . .	22
4.1	The three rooms used in this study. . . . .	26

4.2	WF step and measurement positions. . . . .	27
4.3	The arc maps obtained by WF in the three rooms. . . . .	28
4.4	BU occupancy probability grids obtained by WF in the three rooms.	29
4.5	The result of applying MP to the arc maps obtained by WF in the three rooms. . . . .	30
4.6	The result of applying VT to the arc maps obtained by WF in the three rooms. . . . .	31
4.7	The result of applying the ATM algorithm to the arc maps obtained by WF in the three rooms. . . . .	32
4.8	The result of applying DM to the arc maps obtained by WF in the three rooms. . . . .	34
4.9	VDs of the three rooms. . . . .	36
4.10	Sampled versions of the VDs indicating the points where measure- ments are taken. . . . .	37
4.11	The arc maps obtained by VD tracing in the three rooms. . . . .	38
4.12	BU occupancy probability grids obtained by VD tracing in the three rooms. . . . .	39
4.13	The result of applying MP to the arc maps obtained by VD tracing in the three rooms. . . . .	40
4.14	The result of applying VT to the arc maps obtained by VD tracing in the three rooms. . . . .	41
4.15	The result of applying the ATM algorithm to the arc maps obtained by VD tracing in the three rooms. . . . .	42



4.16	The result of applying DM to the arc maps obtained by VD tracing in the three rooms. . . . .	43
A.1	Geometry of the problem with the given sensor pair when the target is a plane (adopted from [1]). . . . .	50
B.1	WF algorithm flowchart. . . . .	54

# List of Tables

3.1	Error criteria for the two simulation examples. . . . .	23
4.1	Mean absolute error – indoor simulations with WF. . . . .	44
4.2	Fill ratio – indoor simulations with WF. . . . .	45
4.3	CPU time – indoor simulations with WF. . . . .	45
4.4	Mean absolute error – indoor simulations with VD tracing. . . . .	45
4.5	Fill ratio – indoor simulations with VD tracing. . . . .	46
4.6	CPU time – indoor simulations with VD tracing. . . . .	46

# Chapter 1

## Introduction

The basic awareness of the surrounding environment is a notable feature of intelligent mobile robots. This awareness can be accomplished by means of simple sensor utilization and processing of obtained sensory data according to the perceptive needs of the robot such as navigation, tracking and/or avoidance of targets, path-planning and localization. In static but unknown environments, where an a priori map of the working area is not available, or in dynamically changing environments, the robot is supposed to build an accurate map of its surroundings by using the sensory data it gathers for autonomous operation. Therefore, the selection of an appropriate map-building scheme is an important issue.

Ultrasonic sensors have been widely utilized in robotic applications due to their accurate range measurements and low cost. The frequency range at which air-borne ultrasonic transducers operate is associated with a large beamwidth that results in angular uncertainty of the echo-producing target. Thus having an intrinsic uncertainty of the actual angular direction of the range measurement and being prone to various phenomena such as multiple and higher-order reflections and cross-talk between transducers, a considerable amount of modeling, processing and interpretation of the sensory data is necessary.

Being a low-cost solution to the sensory perception problem with robust characteristics, ultrasonic sensors have been widely used in map-building applications [2,3].

Grid-based and feature-based approaches have been in use to represent the environment since the early days of map building. The occupancy grids were introduced in [4] and a Bayesian update scheme for cell occupancy probabilities was suggested. In [5], a dynamic map-building method via correlating fixed beacons was developed and map building in dynamic environments has been investigated in a number of studies [6, 7].

As an alternative to grid-based approaches to map building and world representation for mobile robots, feature-based approaches have also been popular [5, 6, 8, 9]. In this school of map representation, the world model is described in terms of natural features of the environment (e.g., planes, corners, edges and cylinders) the orientation and position of which are known [10, 11]. The echo patterns of planes, corners and edges were first modeled in [10] and they have been used as natural beacons for map building in [6]. Planes and corners were differentiated by using the amplitude and time-of-flight characteristics of the ultrasonic data [11]. In [12] and [13], the complete waveform of the received echo is processed using matched filters in order to achieve higher accuracy. In [14], maximum likelihood estimation is employed in a 3-D setting. Evidential reasoning was utilized in [1] in a multi-sensor fusion application. In addition to map-building applications of ultrasonic target differentiation, it was reported in [15] that an ultrasonic sensor mounted at the tip of a robot arm could be used to differentiate coins and O-rings.

Map-building applications can also be classified according to the coverage scheme employed. The systematic way the unknown environment to be mapped is covered, or motion planning, may be roughly divided into three approaches. One method of ground coverage scheme involves pseudo-random steps with collision avoidance [16–18]. The more systematic wall following type coverage can further be divided into two general cases: simple rule-based wall following [19] and potential field-based wall following [20]. In the second case, each obstacle/wall creates a potential field and the mobile platform aims at staying on constant potential lines. There also exist different approaches to the wall-following problem that cannot be included under the above two categories [21, 22], for example, those which employ fuzzy-logic based control methods [23]. The third and most sophisticated coverage scheme involved in map building is based on Voronoi diagrams that can be constructed

iteratively [24–26].

The main contribution of this thesis is that it provides a valuable comparison between the performances of one newly proposed and four existing algorithms for processing ultrasonic arc maps for map-building purposes. The comparison is based on three different error criteria. Each method is found to have certain advantages and disadvantages which make them suitable for map building under different constraints and requirements. The newly proposed method is promising as it introduces a sense of direction in the data acquisition and processing. This is found to be beneficial and the determination of such directional awareness is proved to be cost-effective since most motion-planning approaches already involve a similar sense of direction. The newly proposed method also results in the minimum mean absolute error between the true map and constructed map. Another contribution of this thesis is the comparison it provides between two different motion-planning schemes which are wall following and Voronoi diagram tracing for map-building applications. Even though the simulation results demonstrated in this thesis are solely based on ultrasonic data and map-building applications, the same approach can conveniently be extended to other sensing modalities such as radar and infrared, as well as other mobile robot applications.

This thesis is organized as follows: In Chapter 2, the basics of ultrasonic sensing are reviewed. Descriptions and a basic comparison of five different map-building techniques are given in Chapter 3, through two simulation examples. Chapter 4 expands the comparison to indoor map-building scenarios. The results are presented and discussed at the end of each chapter with numerical success measures, while final notes, conclusions, and future work form Chapter 5.

# Chapter 2

## Basics of Ultrasonic Sensing

This chapter reviews the basics of ultrasonic sensing, in particular, time-of-flight (TOF) measurement using ultrasonic sensors. Operating principles, governing equations and uncertainties related to ultrasonic sensors are summarized.

### 2.1 Ultrasonic Transducers

Ultrasonic sensors operate at frequencies between 20–300 kHz. They perform transduction by converting electrical signals to acoustical waves and converting the received reflection of the transmitted waves back into electrical signals. Acoustical waves transmitted by the transducer exhibit different characteristics in the near field, where *Fresnel diffraction* is dominant, and the far field, where *Fraunhofer diffraction* is dominant. According to the harmonically vibrating circular piston model of the transducer in the near field [27], the beam is confined to a cylinder with radius  $a$ , which is the radius of the transducer aperture. The length of this field is  $r_{min} = \frac{(4a^2 - \lambda^2)}{4\lambda} \cong \frac{a^2}{\lambda}$  from the face of the transducer where  $\lambda$  is the wavelength of the acoustic transmission. On the other hand, the beam is confined to a cone with angle  $2\theta_0$  in the far field. We are mainly interested in the far field since the range measurements of interest correspond to this region and the complexity of the acoustical interference is high in the near field [27].

The far-field pressure amplitude of an ultrasonic pulse transmitted *at a single frequency* is given by the following formula [28]:

$$A(r, \theta) = A_0 \frac{r_{min}}{r} \frac{J_1(ka \sin \theta)}{ka \sin \theta} \quad \text{for } r \geq r_{min} \quad (2.1)$$

where  $r$  stands for the radial distance from the transducer,  $\theta$  for the angular deviation from the line-of-sight (LOS),  $k$  for the wavenumber ( $k = 2\pi/\lambda$ ),  $A_0$  for the pressure amplitude at the near-field/far-field interface on the LOS and the function  $J_1$  for the first-order Bessel function of the first kind.

At constant range  $r$ , the pressure amplitude of the acoustical waves given in Equation (2.1) becomes only a function of  $\theta$ . This  $\theta$  dependency is dominated by the Bessel function divided by  $ka \sin \theta$ , and the zeroes of the Bessel function determines the zeroes of the pressure amplitude at constant  $r$ , creating the lobes of the beam pattern, within which the acoustical energy is confined. First of these zeroes is located at  $ka \sin \theta_0 = 1.22\pi$ , which corresponds to:

$$\theta_0 = \sin^{-1} \left( \frac{1.22\pi}{ka} \right) = \sin^{-1} \left( \frac{0.61\lambda}{a} \right) \quad (2.2)$$

where  $\theta_0$  is called the *half-beamwidth angle* that marks the ends of the main lobe, which in turn represents the approximate beamwidth of the device. The secondary or side lobes are neglected, since a considerable portion of the acoustical energy is confined within the main lobe.

The pressure amplitude pattern of the transducer in the far field is composed of a range of frequencies centered around the resonance frequency  $f_0$ , and can be modeled as a Gaussian resulting from the superposition of multiple Bessel functions [28]:

$$A(r, \theta) = A_0 \frac{r_{min}}{r} \exp \left( -\frac{\theta^2}{2\sigma_T^2} \right) \quad \text{for } r \geq r_{min} \quad (2.3)$$

where the standard deviation of the Gaussian is related to the sensor beamwidth by  $\sigma_T = \theta_0/2$  [1]. The echo of the transmitted beam pattern from a planar reflector when the transmitter and receiver are separate devices, is given as follows:

$$A(r_1, r_2, \theta_1, \theta_2) = A_{max} \frac{2r_{min}}{r_1 + r_2} \exp \left[ \frac{-(\theta_1^2 + \theta_2^2)}{2\sigma_T^2} \right] \quad \text{for } r_1, r_2 \geq r_{min} \quad (2.4)$$

where  $\theta_1$  and  $\theta_2$  are the angles, and  $r_1$  and  $r_2$  are the distances of the surface to the transmitter and the receiver respectively. Please refer to Figure A.1 in Appendix A for an illustration of the geometry.  $A_{max}$  is the maximum amplitude obtained when the transmitter and receiver are coincident and  $\theta_1 = \theta_2 = 0^\circ$  and  $r_1 = r_2 = r_{min}$  [28].

## 2.2 Ultrasonic Time-of-Flight Measurement

In this thesis, we employ time-of-flight (TOF) based ultrasonic range measurement. The TOF is defined as the round-trip travel time of the ultrasonic pulse from the time it is transmitted from the transducer to the time its reflection echo from a surface is received. If the same transducer functions as both transmitter and receiver, the device operates in the *monostatic* mode [29]. On the other hand, if the transmitter and receiver are different devices, the operation mode is *bistatic*.

In earlier work, it has been shown that the reflected signals are well approximated by a sinusoid with a Gaussian envelope [10]:

$$A(r, \theta, t) = A_{max} \frac{r_{min}}{r} \exp \left( \frac{-\theta^2}{2\sigma_T^2} \right) \exp \left[ \frac{-(t - t_0 - t_d)^2}{2\sigma^2} \right] \sin[2\pi f_0(t - t_0)] \quad (2.5)$$

where  $f_0$  is the resonance frequency,  $t_0$  is the TOF,  $t_d$  is the time shift between the beginning and the peak of the Gaussian envelope and  $\sigma$  is the standard deviation of the Gaussian signal envelope.

The received signal model is illustrated in Figure 2.1. The echo is usually contaminated by noise and the time at which the reflection is received can be determined by means of *simple thresholding*, using a constant threshold level. The true value of the TOF corresponds to the starting point of the echo. Simple thresholding results in a biased TOF estimate, since the threshold is usually exceeded a little bit later than the starting point so that the estimated TOF is slightly larger than the actual. If



the threshold is set too low, there will be many false echo detections due to the noise on the signal. On the other hand, if it is set too high, the bias in the TOF estimates increases and it is possible to miss some of the weaker echoes with low amplitude. Hence, there is a trade-off between the false detection rate and missed detection rate of echoes. Assuming a zero-mean Gaussian additive noise model, the threshold level is usually set to 4–5 standard deviations of the noise, since Gaussian noise will remain within  $\pm 3$  standard deviations of the mean 99.73% of the time [30]. In the given example in Figure 2.1,  $\sigma = 0.001$  sec,  $t_d = \frac{3}{f_0}$ ,  $\theta = 0^\circ$  and the additive noise is zero-mean Gaussian with a standard deviation of 0.005. The threshold level was set equal to five standard deviations of the noise which is 0.025, resulting in some bias on the measurements but reducing the rate of false echo detections. The true TOF value was 11.66 ms, and the TOF estimate was 11.68 ms. In order to reduce or eliminate the bias, alternatives to simple thresholding such as adaptive, variable or double thresholding [31] and curve-fitting [32] techniques have been proposed.

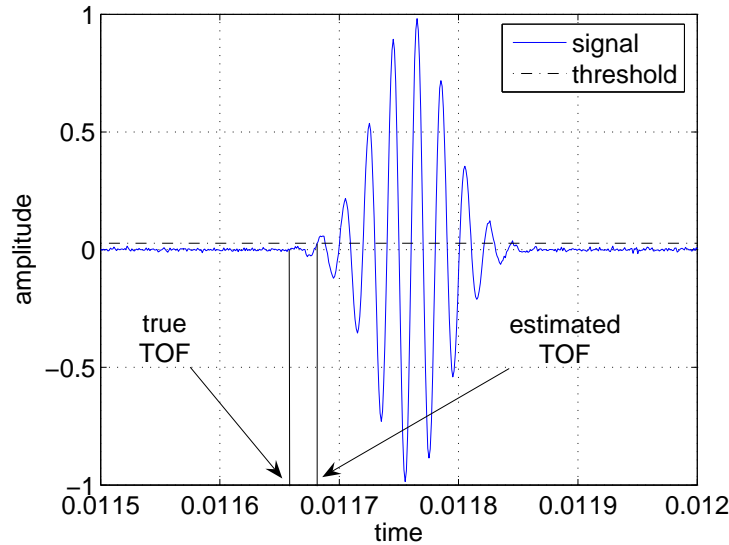


Figure 2.1: Typical received echo with additive noise and the threshold level.

Once the TOF value is estimated, the range can be easily calculated from

$$r = \frac{c t_0}{2}, \quad (2.6)$$

where  $t_0$  represents the TOF and  $c$ , the speed of sound is given by

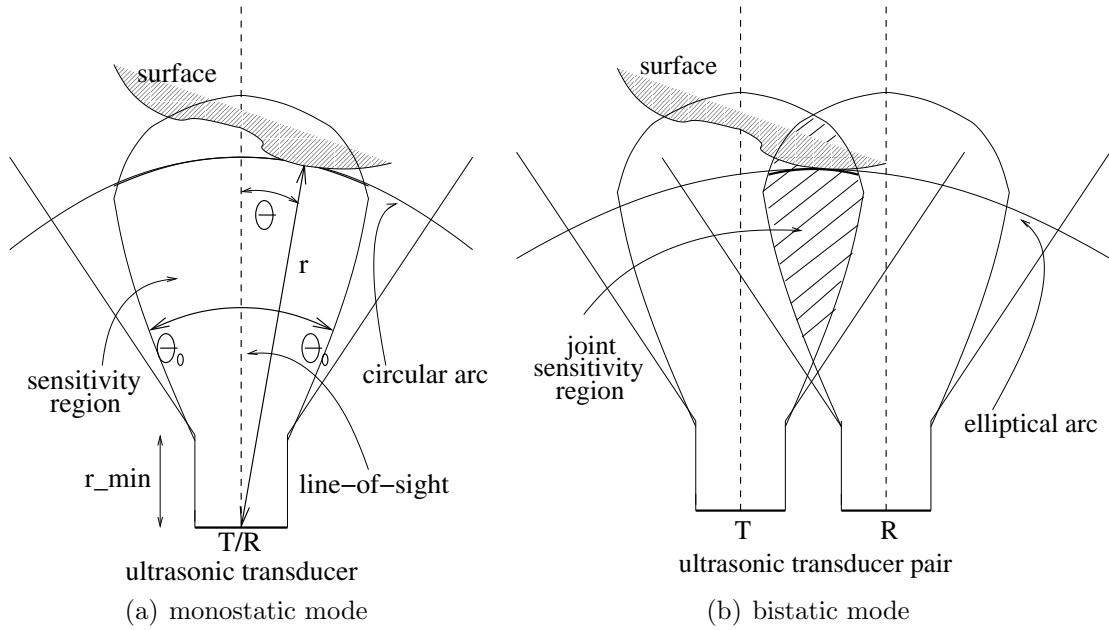


Figure 2.2: (a) Single transducer configuration resulting in a *circular* arc, (b) dual transceiver configuration resulting in an *elliptical* arc.

$$c = 331.4\sqrt{T/273} \text{ m/s} = 343.3 \text{ m/s at room temperature } (T = 293 \text{ K}).$$

Since most air-borne ultrasonic sensing systems operate below a resonance frequency of 200 kHz, frequencies involved correspond to wavelengths well above several millimeters, and the reflection from the measured surface is specular, not diffused. Due to this mirror-like reflection, when the transducer is operated in the monostatic mode (Figure 2.2(a)), an echo can be detected only if the incoming ray is perpendicular to the surface at some point. In the bistatic mode (Figure 2.2(b)), there should be a path between the transmitter and receiver such that at the point of reflection, the angle of incidence and the angle of reflection made with the surface normal are equal.

## 2.3 Representing Angular Uncertainty by Arc Maps

In this study, simple ultrasonic range sensors are modeled that measure the TOF and provide a range measurement according to Equation (2.6). Although such devices return accurate range data, typically they cannot provide direct information on the angular position of the point on the surface from which the reflection was obtained. Most commonly, the large beamwidth of the transducer is accepted as a device limitation that determines the angular resolving power of the system, and the reflection point is assumed to be along the LOS. According to this naive approach, a simple mark is placed along the LOS of the transducer at the measured range, resulting in inaccurate maps with large angular errors. Alternatively, the angular uncertainty in the range measurements has been represented by *regions of constant depth* [33] and ultrasonic *arc maps* [34,35] that represent the angular uncertainty while preserving more information. This is done by drawing arcs spanning the beamwidth of the sensor at the measured range, representing the angular uncertainty of the object location and indicating that the echo-producing object can lie anywhere on the arc. Thus, when the same transducer transmits and receives, all that is known is that the reflection point lies on a circular arc of radius  $r$ , as illustrated in Figure 2.2(a). More generally, when one transducer transmits and another receives, it is known that the reflection point lies on the arc of an ellipse whose focal points are the transmitting and receiving elements (Figure 2.2(b)). The arcs are tangent to the reflecting surface at the actual point(s) of reflection. Arc segments near the actual reflection points tend to reinforce each other. Arc segments not actually corresponding to any reflections and simply representing the angular uncertainty of the transducers remain more sparse and isolated. Similarly, those arcs caused by higher-order reflections, crosstalk, and noise also remain sparse and lack reinforcement. By combining the information inherent in a large number of such arcs, angular resolution far exceeding the beamwidth is obtained.

Apart from the wide beamwidth, another commonly noted disadvantage of ultrasonic range sensors is the difficulty associated with interpreting spurious readings, crosstalk, higher-order, and multiple reflections. The proposed method is capable of

effectively suppressing the first three of these, and, although not implemented here, it would have the intrinsic ability to process echoes returning from surface features further away than the nearest (i.e., multiple reflections) informatively.

The device that is modeled and used in this study is the Polaroid 6500 series transducer [36] operating at a resonance frequency of  $f_0 = 49.4$  kHz, corresponding to a wavelength of  $\lambda = c/f_0 = 6.9$  mm. The half beamwidth of the transducer is  $\theta_0 = \pm 12.5^\circ$ , the transducer aperture radius is  $a = 2$  cm and  $r_{min} = 5.7$  cm. We use a pair of these transducers, with a center-to-center separation of 9 cm. Each transducer is fired in sequence and both transducers detect the resulting echoes. After a pulse is transmitted, if echoes are detected at both transducers, this corresponds to one circular and one elliptical arc. Hence, with two transducers each firing in its own turn, at most four arcs are obtained at each position of the transducer pair. The signal models of these echoes are provided in Appendix A.

In the following chapters, we introduce a new method to process these arc maps and compare it with the existing methods.

# Chapter 3

## Algorithm Descriptions

In this work, we implemented and compared the following algorithms for processing arc maps, the last of which is developed in this thesis:

- Bayesian update scheme [3],
- morphological processing of arc maps [34, 35],
- voting and thresholding of arc maps [37, 38],
- arc-transversal median algorithm [39],
- and directional maximum algorithm.

Different arc maps, each corresponding to a certain set of TOF measurements is processed by each method and the results are compared.

### 3.1 Bayesian Update (BU)

Occupancy grids representing the probability of occupancy are introduced primarily by Elfes and Moravec [3, 4]. A Bayesian update scheme for these occupancy

grids by using ultrasonic sensor data was suggested in [3] and is included in this thesis as an earlier example of related work. Starting with a blank or completely uncertain occupancy grid, each range measurement updates the grid formation in a Bayesian manner. For a certain measurement, the following sensor characteristics and obtained data are listed for each pixel  $P(x, y)$  of the map to be updated:

- $r$  range measurement returned by the ultrasonic sensor
- $r_{min}$  lower range threshold (near-field limit)
- $r_\epsilon$  maximum ultrasonic range measurement error
- $\theta_0$  sensor half-beamwidth angle
- $2\theta_0$  beamwidth angle subtending the main lobe of the sensitivity region
- $S = (x_s, y_s)$  position of the ultrasonic sensor
- $\sigma$  distance from  $P(x, y)$  to  $S = (x_s, y_s)$

Occupancy probability of the scanned pixels are defined over two distinct probability measures: ( $p_E$ , probability of emptiness and  $p_O$ , probability of occupancy). These probability density functions are defined as follows:

$$\begin{aligned} p_E(x, y) &= p[\text{point } (x, y) \text{ is empty}] \\ &= E_r(\sigma) \cdot E_a(\theta) \end{aligned}$$

where  $E_r(\sigma)$  and  $E_a(\theta)$  are respectively the range and angle dependency of the probability density function for emptiness, given by:

$$E_r(\sigma) = \begin{cases} 1 - [(\sigma - r_{min}) / (r - r_\epsilon - r_{min})]^2 & \text{for } \sigma \in [r_{min}, r - r_\epsilon], \\ 0 & \text{otherwise,} \end{cases}$$

and

$$E_a(\theta) = 1 - (\theta/\theta_0)^2, \text{ for } \theta \in [-\theta_0, \theta_0].$$

Likewise,  $p_O$  is defined as:

$$\begin{aligned} p_O(x, y) &= p[\text{position } (x, y) \text{ is occupied}] \\ &= O_r(\sigma) \cdot O_a(\theta) \end{aligned}$$

where  $O_r(\sigma)$  and  $O_a(\theta)$  are respectively the range and angle dependency of the probability density function for occupancy, and defined as:

$$O_r(\sigma) = \begin{cases} 1 - [(\sigma - r)/r_\epsilon]^2, & \text{for } \sigma \in [r - r_\epsilon, r + r_\epsilon] \\ 0 & \text{otherwise,} \end{cases}$$

and

$$O_a(\theta) = 1 - (\theta/\theta_0)^2, \text{ for } \theta \in [-\theta_0, \theta_0].$$

The  $p_E$  and  $p_O$  described above are illustrated in Figure 3.1.

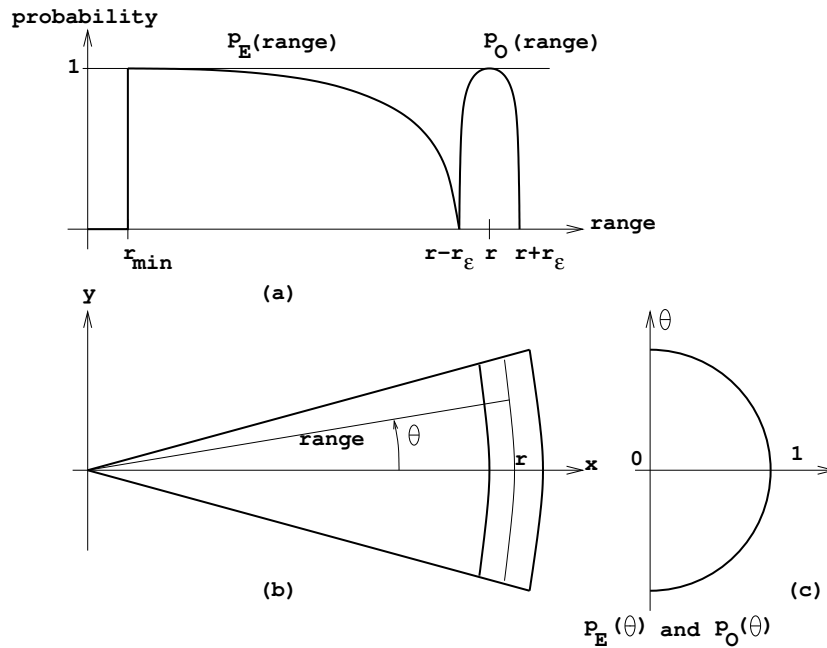


Figure 3.1: (a) Range dependency, (b)  $x$  and  $y$  dependency, and (c)  $\theta$  dependency of  $p_O$  and  $p_E$ .

The algorithm starts with an initially uncertain map where all the pixel values are set to zero which corresponds to the mid-point of the interval  $[-1, 1]$  for pixel

values. For each range measurement,  $p_E$  and  $p_O$  values are calculated for the cells inside the field of view of the transducer by using the above formulas. The following Bayesian update rules are used to update the existing values in the cell array:

$$p_E(\text{cell}) := p_E(\text{cell}) + p_E(\text{reading}) - p_E(\text{cell}) \times p_E(\text{reading})$$

$$p_O(\text{cell}) := p_O(\text{cell}) + p_O(\text{reading}) - p_O(\text{cell}) \times p_O(\text{reading})$$

The map of the environment is built by iteratively updating the contents of each cell via a number of range measurements. In the end,  $p_E$  and  $p_O$  arrays form modified probability distribution functions that vary between  $-1$  and  $1$ .

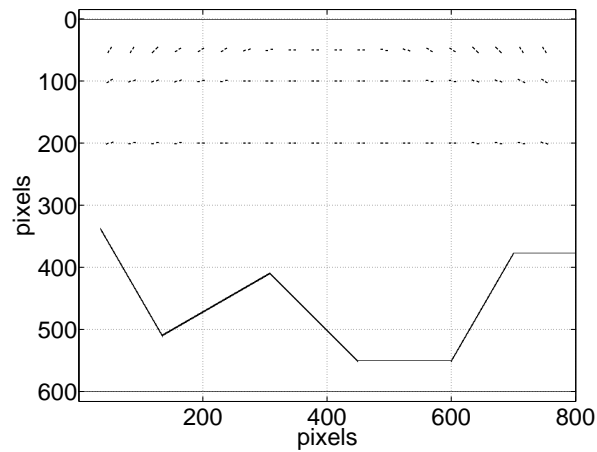


Figure 3.2: Simulation example 1 – actual surface profile and the transducer positions.

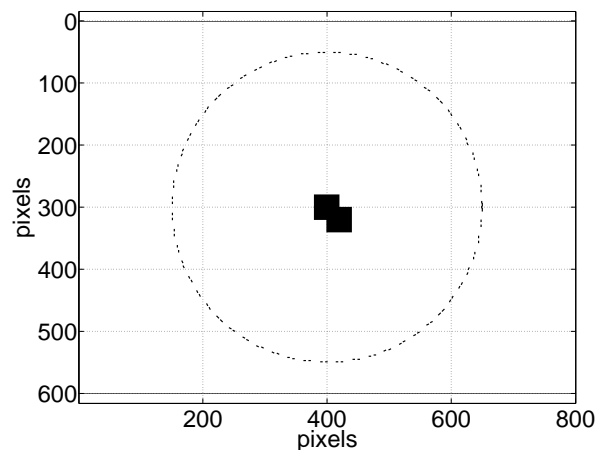


Figure 3.3: Simulation example 2 – actual object and the transducer positions.



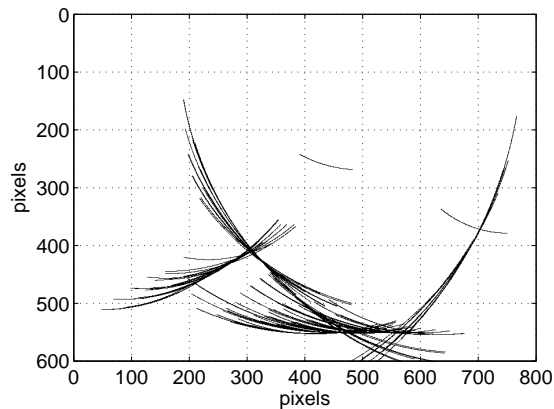
The algorithm is implemented and demonstrated by two different simulation examples first. In the first case, a piece-wise linear surface profile is simulated (Figure 3.2). In the second case, an angular scanner is simulated, in which an object shown in Figure 3.3 is scanned. In the first case, or example 1, the transducer pairs with a center-to-center separation of 9 cm are regularly located in three rows, uniformly distributed in each row, 50 cm between the first two rows and 1 m between the second and the third rows, the third row being the closest one to the surface. The transducer pairs in the first row have a regular LOS sweep along the line starting from  $330^\circ$  and ending on the rightmost end at  $210^\circ$ , the second row has a sweep from  $300^\circ$  to  $240^\circ$  and the third row has a sweep of  $290^\circ$  to  $250^\circ$ , all angles being measured from the  $+x$  axis. For the angular scanner setting, or example 2, transducer pairs are regularly distributed on a circle, at a constant distance of 250 cm from the object to be scanned. The transducers are radially oriented and looking inward. A total of 120 transducer positions are used in each case, corresponding to 60 different positions of the transducer pair and at most 240 arcs in the arc map. The resulting arc maps for each simulation example can be seen in Figure 3.4.

The rays within the beamwidth of the transducer are modeled from  $-12.5^\circ$  to  $+12.5^\circ$  at  $0.5^\circ$  intervals. Assuming specular reflections, perpendicular incidence of each ray with the predefined world array is checked. If such an incidence is found, then the round trip distance is calculated and actual thresholding delay of the ultrasonic circuitry is accounted for by thresholding a shifted Gaussian-modulated sinusoid.

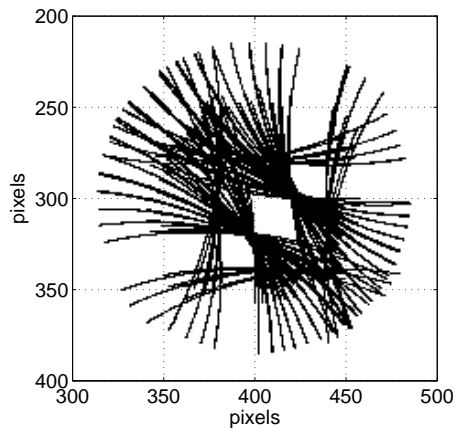
For the case where there are multiple reflections from the field of view of a transducer after a single transmission, the very first echo is registered, as the first echo to trigger the transducer is assumed to be from the obstacle with the minimum distance to the transducer.

The world model in each example consists of a 2-D array of  $800 \times 600$  elements. Each element (further referred as a “pixel”) contains a double value with which we can represent either occupancy or a weight/probability of occupancy. Similar occupancy grid applications are first suggested by Elfes and Moravec and have been widely popular [40, 41].

In computer simulations, MATLAB is chosen as the coding platform, mainly due to the ease of mathematical description, visual representation efficiency and relative familiarity. Faster programming platforms, such as Visual C++ can be deployed, if and when the computational complexity of the algorithms become demanding. The .m files of the MATLAB code can be found in Appendix C.



(a) example 1 arc map



(b) example 2 arc map

Figure 3.4: Arc maps of the two simulation examples.

The surface profile in Figure 3.5 is obtained by using the algorithm described above on the example given in Figure 3.2. The only modification done to the original algorithm given in [3] is that besides the circular arcs, the elliptical crosstalk arcs described in Chapter 2 are also included for a fair comparison with the other algorithms, by including (at most) four probability density updates for each position

of the transducer pair, corresponding to four arcs drawn in the arc map. As seen in Figure 3.5, the resultant map contains a considerable amount of artifacts and further cleaning is required in order to obtain a useful representation of the actual profile.

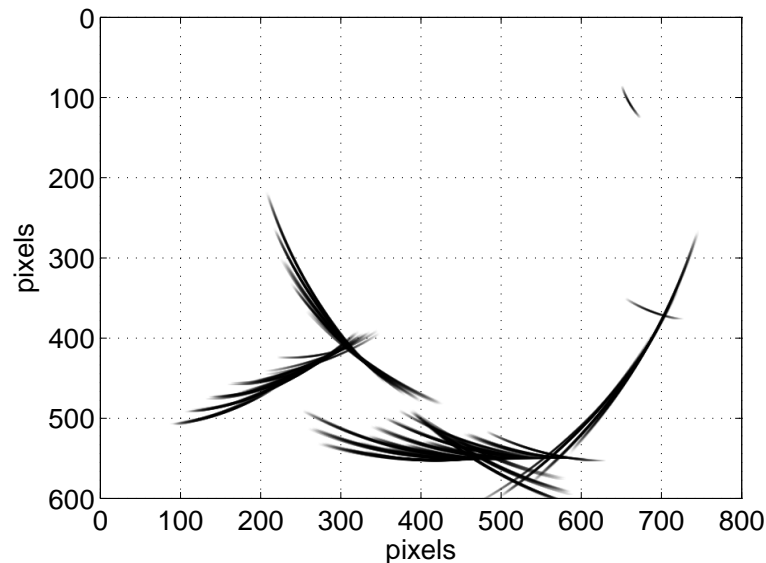


Figure 3.5: Example 1 – BU result for occupancy probabilities.

## 3.2 Morphological Processing (MP)

Morphological processing techniques have been used in pattern recognition applications since they were first introduced [42]. Erosion, dilation, opening, closing, thinning and pruning are the fundamental binary morphological operations, and the use of these techniques was extended even to gray-scale images [43]. Being easy-to-use yet powerful tools in image processing, morphological operators have widely been employed in a number of areas including biomedical engineering, machine vision and remote sensing. In addition to conventional images, range data have also been processed by morphological operators [44] and the processing of ultrasound data from medical applications was explored in [45].

The processing of ultrasonic arc maps using morphological processing techniques was first proposed by Başkent and Barshan [34]. Morphological processing of arc maps defines an easy to implement, yet effective solution to ultrasonic map building. The arc map usually has artifacts that can be due to higher-order reflections, erroneous readings or noise. Luckily, these are not enhanced as much as the arcs resulting from the actual surface profile. By applying binary morphological processing operations, one can eliminate the artifacts of the arc map and extract the surface profile. In the study reported in [34], a large number of transducers was used, configured linearly, circularly or randomly. The best results were obtained with the randomly distributed configuration. The main problem with this technique was that the method did not perform so well where the curvature of the surface changes sharply, such as at corners and edges. In our case, opening operation (erosion followed by dilation) is applied to the arc map at hand for the two simulation examples. The details of the simulations are as described in Section 3.1. The morphologically processed result for the first simulation setting (example 1) described there can be seen in Figure 3.6.

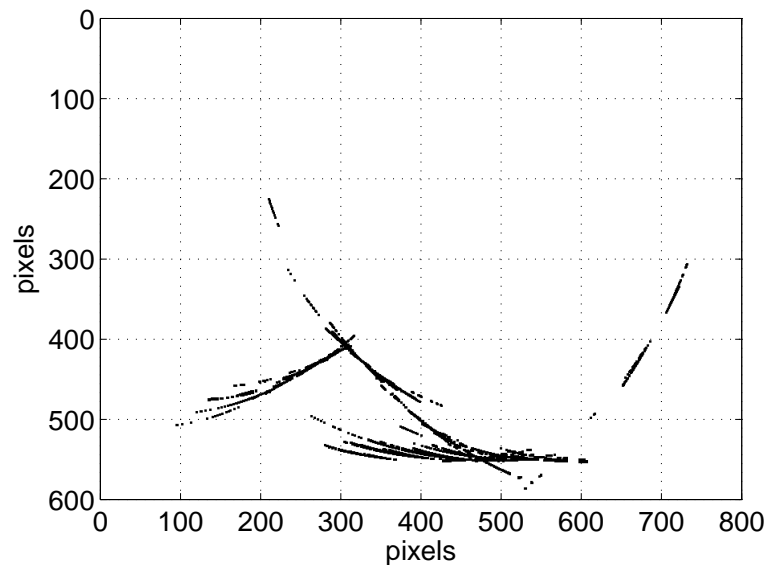


Figure 3.6: Example 1 – MP results (opening applied).

The artifacts of the raw arc map of Figure 3.4(a) are considerably cleared in

Figure 3.6. However, the corners are still distorted while edges have major discontinuities.

### 3.3 Voting and Thresholding (VT)

An alternative to morphological processing techniques for arc maps is a voting scheme where each pixel holds the number of arcs crossing that pixel, hence having an occupancy weight array of pixels [37,38]. By simply thresholding this array, i.e., zeroing the pixels that have a value lower than a suitable threshold value, artifacts of the arcs can be eliminated and the profile is extracted. A comparison of this approach with morphological processing is provided in [37]. The result of applying this approach to the angular scanner example of Figure 3.3 with a threshold value of five is given in Figure 3.7.

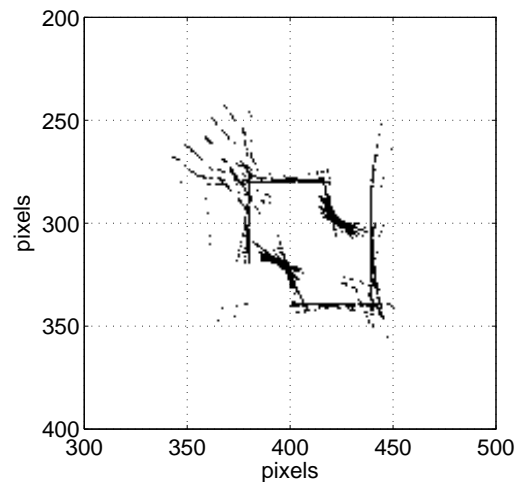


Figure 3.7: Example 2 – VT with a threshold of 5.

While the profile obtained by using VT has some minor point artifacts that cannot be removed without a higher threshold that in turn would cause gaps in the necessary parts of the profile, the overall performance observed in Figure 3.7 is acceptable and the slight inaccuracy at the edges and corners is due to the inherently low angular resolution of the ultrasonic transducer.

### 3.4 Arc-Transversal Median (ATM)

The Arc-Transversal Median Algorithm is a multi-stage approach that requires both extensive bookkeeping and considerable processing [39]. The algorithm can be summarized as follows. For each arc in the arc map, the intersection(s) with other arcs, if they exist, are recorded. For the arcs with intersection(s), the median of the intersection points with other arcs is selected as the actual point of reflection. For the arcs without any intersections, the center-of-line approach is utilized, i.e., the mid-point of the arc is chosen as the actual point of reflection. Hence, this is an algorithm that defines a single point in the map for each ultrasonic echo. It can be considered as a much improved version of the naive approach where a single mark is placed along the LOS at the measured range, which was mentioned in Section 2.3. The angular scanner simulation of example 2 resulted in the profile in Figure 3.8 when the ATM algorithm is applied.

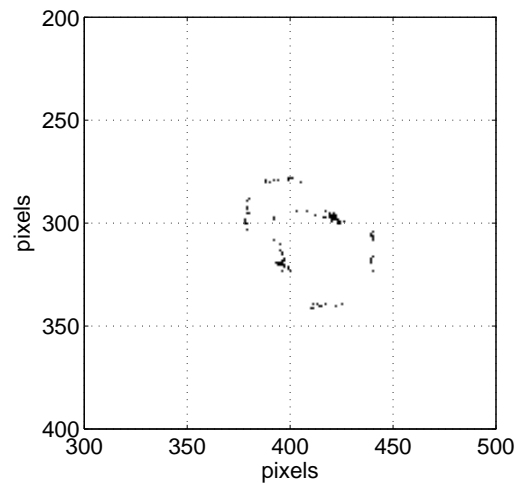


Figure 3.8: Example 2 – ATM.

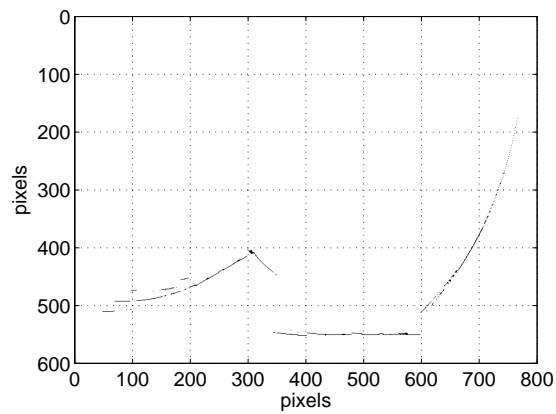
ATM result represented in Figure 3.8 is too sparsely populated and cannot give a useful description of the object. This method also seems to round off edges and results in gaps at the corners.

### 3.5 Directional Maximum (DM)

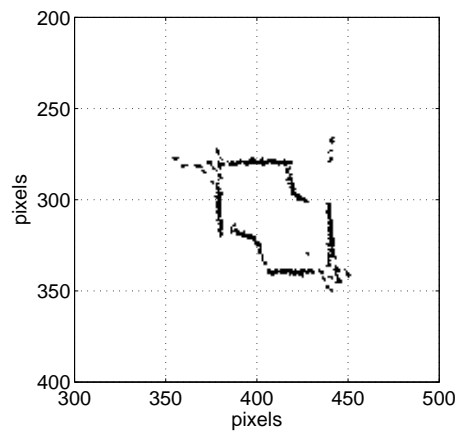
In this method, we assume that we have a designated direction-of-interest (DOI) in any map-building scenario. This direction may be based on prior knowledge, or it can be predetermined by the map-building procedure as demonstrated in the indoor map-building examples in the following chapter. For instance, in our profile determination scenario (example 1), the vertical direction is the DOI, while in the angular scanner case the DOI is the radial direction, which changes as the angular position of the scanner head changes. If DOI is not known, it can be found from the distribution of the data and is chosen perpendicular to the direction along which the spread of the collected data is maximum.

Once the DOI is given or determined, the arc map that contains the artifacts is scanned along this DOI; column-wise for the indoor profile case and radial direction-wise for the angular scanner case. Each column/directional array is processed as to leave only the directional maximum value and blank-out the rest of the pixels. If there exist more than one pixel with the maximum value in the array, the algorithm selects the one encountered first in the DOI. This step constitutes the actual artifact removal step of the algorithm. As a final step, morphological processing is applied to the arc maps of these two examples, consisting of applying the bridging and dilation operations twice.

As seen in Figure 3.9, directional maximum gives cleaner results for both examples, yet the corners of both cases are not fully represented and the edges seem to be slightly discontinuous. The highly populated arc map of example 2 seen in Figure 3.4(b) is successfully cleaned to give a considerably accurate object profile, and the discontinuities of example 1 result are minimal with respect to the other methods. Note that the possible problem of the existence of multiple maxima in a directional array does not occur in these examples.



(a) example 1 result



(b) example 2 result

Figure 3.9: DM results on the two examples.



### 3.6 Results of Simulation Examples

We have defined three distinct error criteria to evaluate and compare the algorithms described above. The first and maybe the more important one is the mean absolute error between the determined and true features. The second error criterion involves the percentile amount of the profile built. The final criterion stands for the computational cost of the algorithms in terms of CPU time. The evaluation of the two simulation examples of this chapter according to these three criteria is given in Table 3.1. These error criteria, one standing for quality, the second for quantity and the last for implementability only make sense when considered together, since putting single perfectly placed pixel on the map is clearly not what we need.

method	mean absolute error (pixels)		fill ratio (percent)		CPU time (sec)	
	example 1	example 2	example 1	example 2	example 1	example 2
BU	19.7	25.3	86.4	100	30.9	32.0
MP	26.4	41.2	72.7	100	0.67	1.35
VT	21.4	22.4	77.3	99.8	<b>0.17</b>	<b>0.20</b>
ATM	<b>6.9</b>	14.0	13.2	45.3	300.3	320.4
DM	20.7	<b>8.4</b>	<b>94.0</b>	<b>100</b>	2.1	7.12

Table 3.1: Error criteria for the two simulation examples.

As can be seen from Table 3.1, ATM, DM and VT each have certain advantages associated. In example 1, ATM produced the least mean absolute error but the processing time associated is much larger than feasible. Processing time of VT is far smaller than the other methods followed by MP and DM. The largest fill ratio is obtained by DM in both examples. DM also has the least mean absolute error in example 2. From the CPU time columns of Table 3.1, DM seems to take longer to compute in the angular scanner scenario (example 2), and this is caused by conversion to polar coordinates before thresholding in order to process along the DOI which is the radial direction in this example and back to Cartesian coordinates afterward. The other algorithms do not need this transformation since they can all operate in Cartesian coordinates.

In this chapter, we have introduced the different techniques compared in this thesis through two simulation examples and defined three error criteria for their

comparison. In the following chapter, the same techniques will be compared in indoor environments using two different approaches for motion planning.

# Chapter 4

## Indoor Mapping Simulations

The algorithms briefly described and demonstrated in the previous chapter are extended into complete indoor mapping simulations in this chapter. Three different environments are modeled whose boundaries are shown in Figure 4.1. Motion planning for ground coverage and map building in unknown environments is implemented in two different ways: wall following and Voronoi diagram tracing.

### 4.1 Wall Following (WF)

The wall-following (WF) scheme utilizes a simple rule-based algorithm, which can be found in Appendix B, to follow the walls at a relatively constant distance. This way, the majority of the total surface profile of the indoor environment is covered. The positions of the “steps” taken by the mobile platform while utilizing the WF algorithm are illustrated using circles in Figure 4.2. While the WF procedure generates these sparsely distributed steps, the actual measurement positions for map building are obtained by interpolating the steps by a factor of ten, taking measurements on nine uniformly distributed points in-between the step positions in addition to the actual step positions. These intermediate points are represented with solid dots in Figure 4.2 for the three rooms. Each of these solid dots corresponds to one of the positions of the transducer pair where TOF measurements are collected.

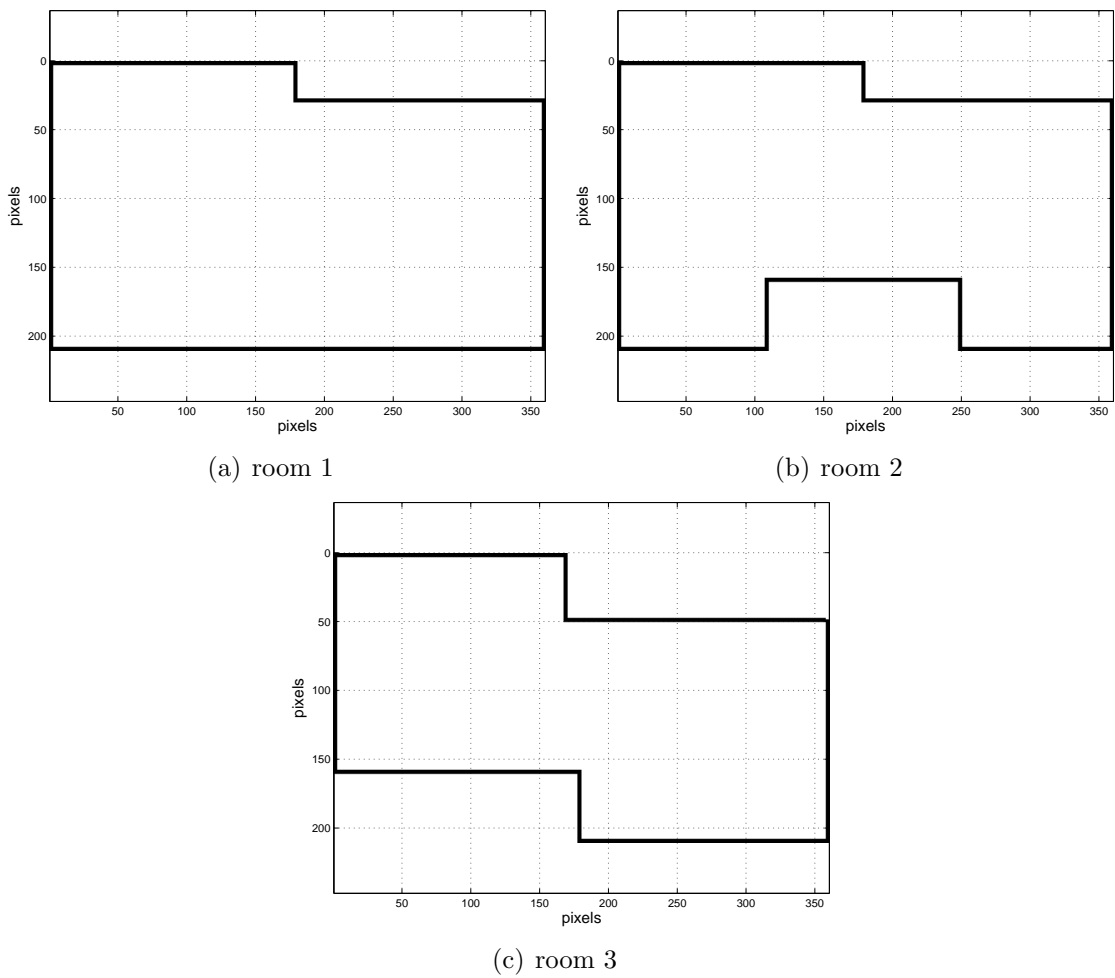
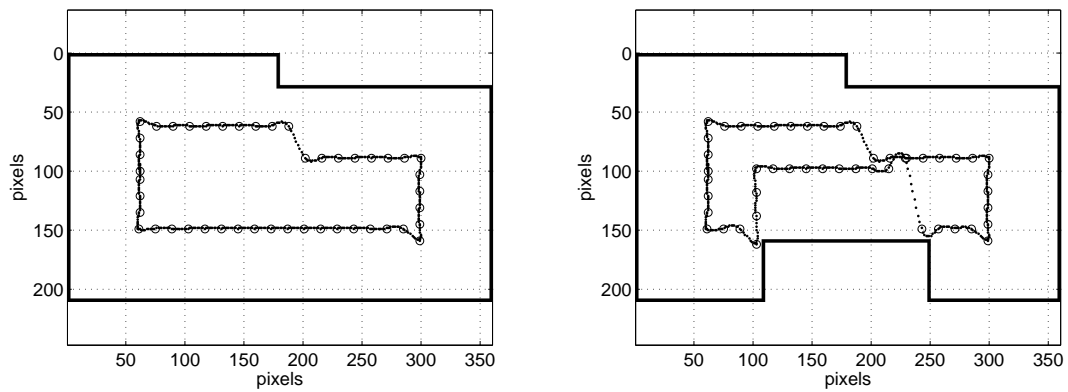
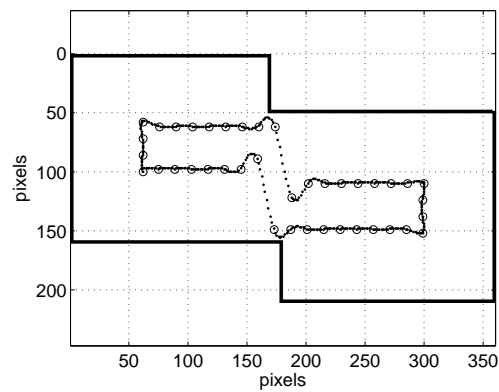


Figure 4.1: The three rooms used in this study.



(a) room 1

(b) room 2



(c) room 3

Figure 4.2: WF step and measurement positions.

In all of the following, transducers placed as a pair in the marked positions fire in sequence, and the resulting echoes are recorded as described in Section 2.3. By using the measurement data taken from the step positions and from the intermediate points in between the actual steps, each of the aforementioned algorithms is executed. The arc maps and the processed maps for each method are given in Figures 4.3–4.6.

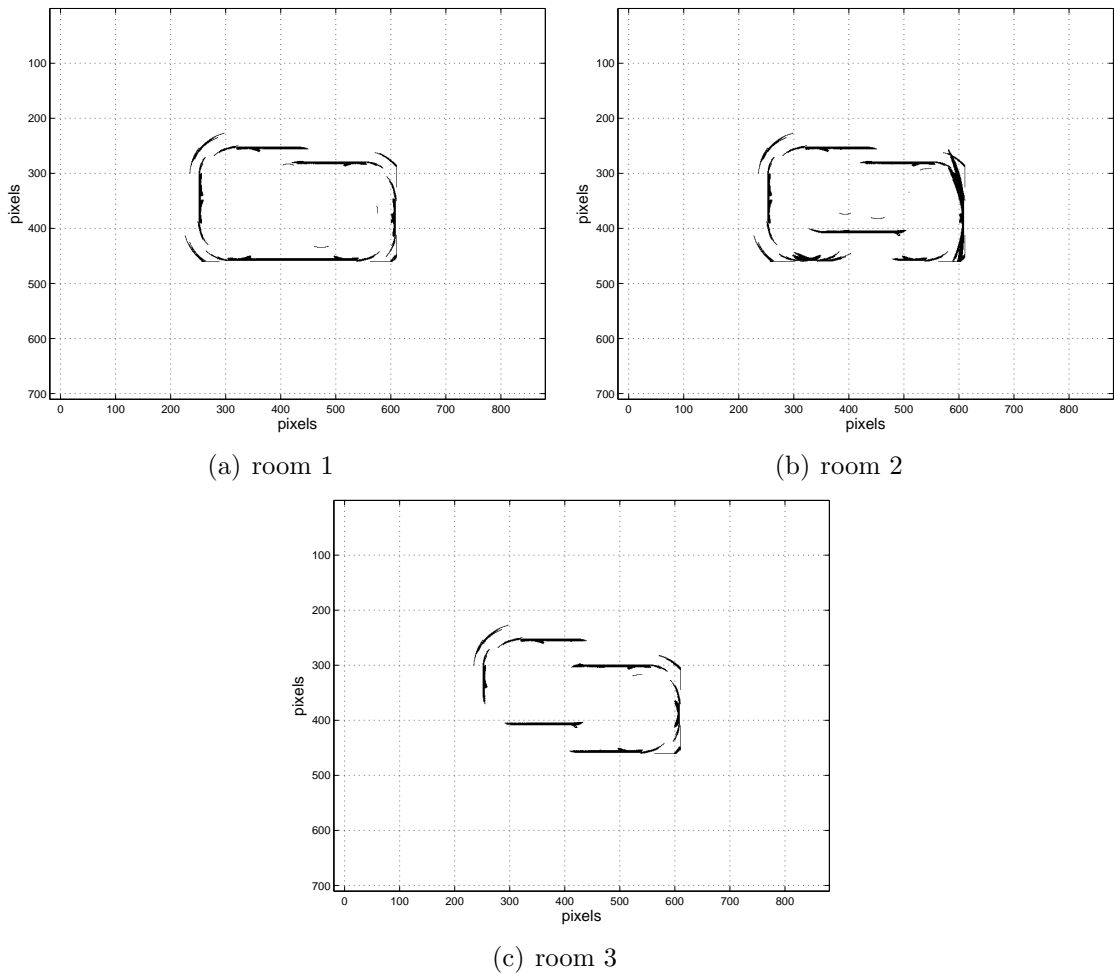


Figure 4.3: The arc maps obtained by WF in the three rooms.

Since WF is a structured method of motion planning, the artifacts of the raw arc maps in Figure 4.3 are minimal, yet there is the need for cleaning the erroneous extensions of planar surfaces, as it is clearly visible in Figure 4.3(b).

### Bayesian Update - WF

The results in Figure 4.4 are obtained by using the WF measurement locations in Figure 4.2 and the Bayesian update scheme.

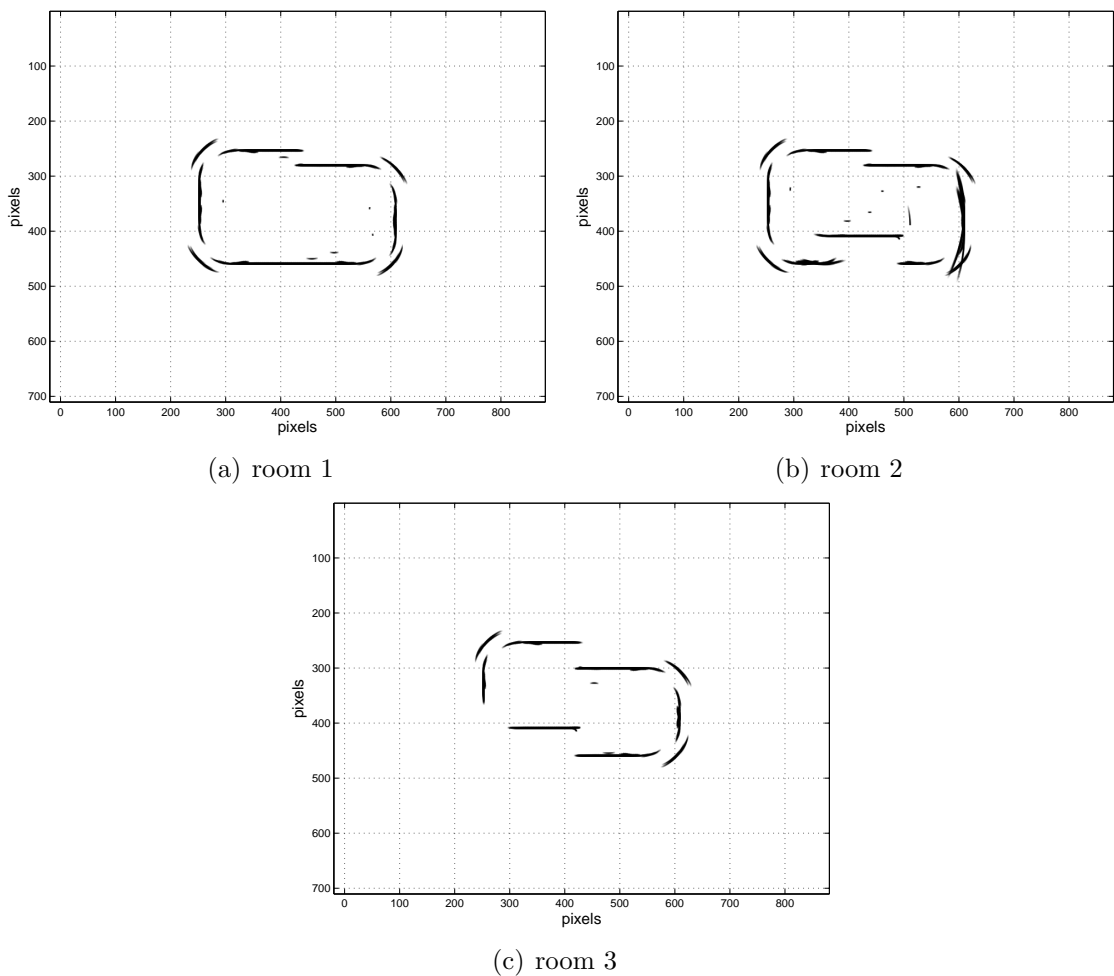


Figure 4.4: BU occupancy probability grids obtained by WF in the three rooms.

Bayesian update, as observed in Figure 4.4, gives a cleaner map for each room, yet the angular uncertainty artifacts and erroneous reading results are still visible, especially for room 2 in Figure 4.4(b).

### Morphological Processing - WF

By applying the thinning operation four times to the arc maps in Figure 4.3, the morphologically processed arc maps in Figure 4.5 are obtained.

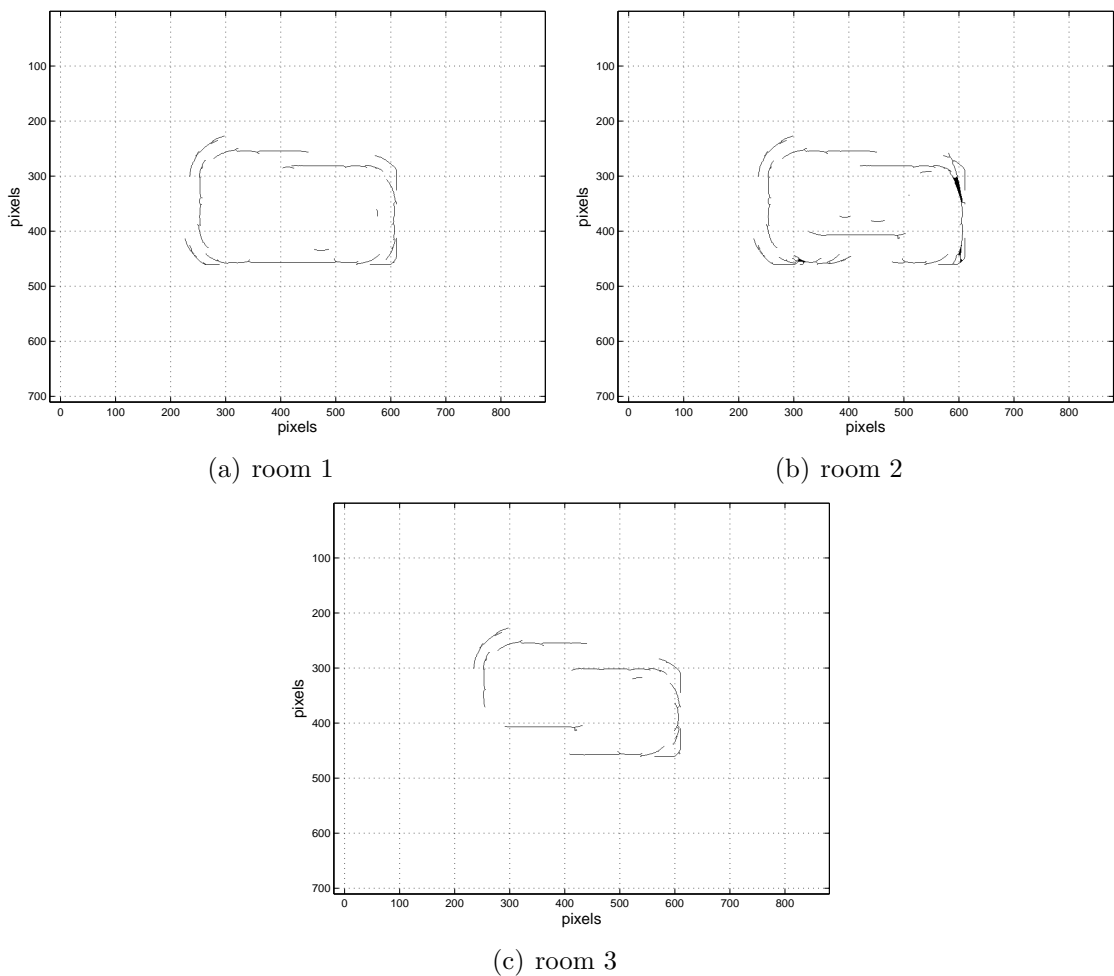


Figure 4.5: The result of applying MP to the arc maps obtained by WF in the three rooms.

Note that a large amount of artifacts has been removed and planar surfaces are satisfactorily represented. However, a substantial amount of branches that clutter the actual map remain and applying further thinning operations not only removes these unwanted branches but also damages the integrity of the map, creating more gaps.



### Voting and Thresholding - WF

By thresholding the arc maps in Figure 4.3 with a threshold value of four, the processed arc maps of Figure 4.6 are obtained.

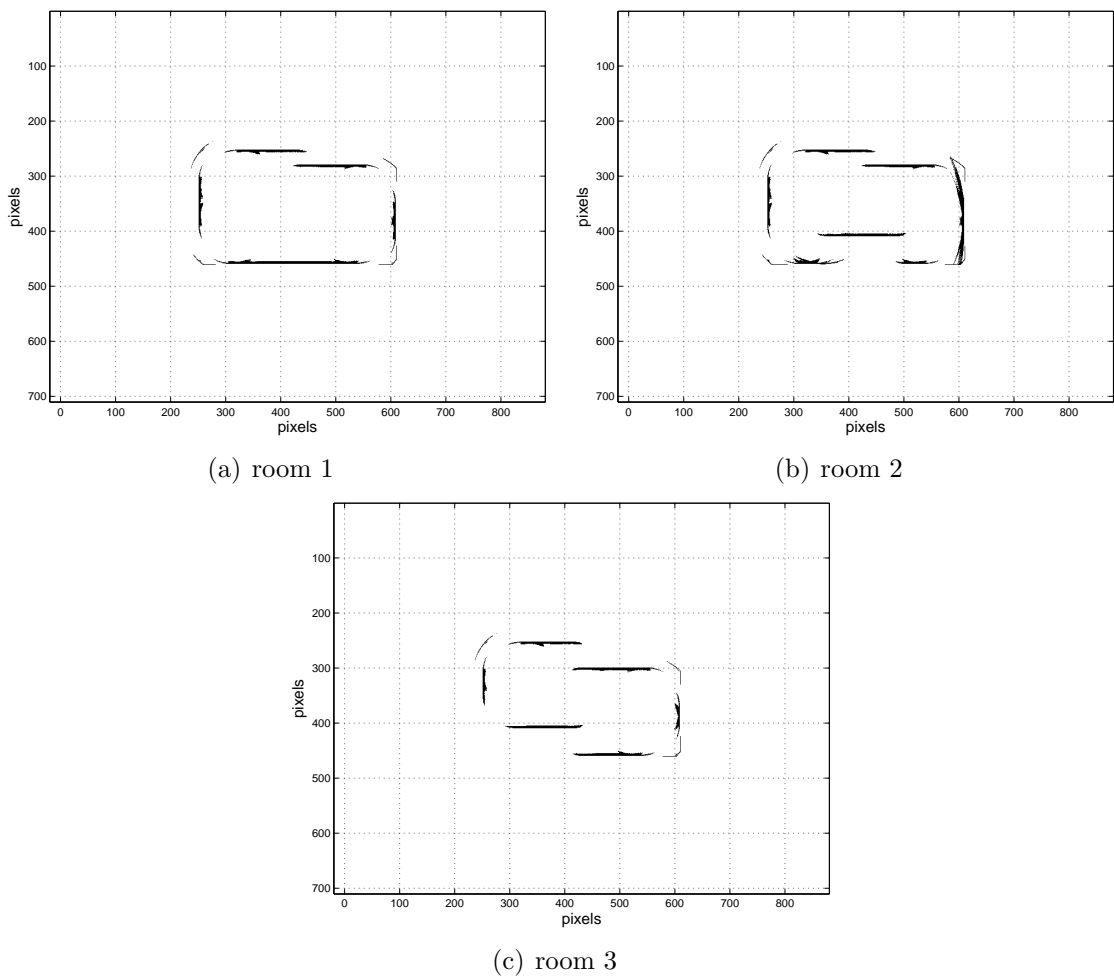


Figure 4.6: The result of applying VT to the arc maps obtained by WF in the three rooms.

This technique still leaves some range uncertainty indicated by thick solid features at planar surfaces, while corners are slightly too much eroded. Less thresholding is found to be prone to a large amount of artifacts while larger thresholds reduce the fill ratios to too low values.

### Arc-Transversal Median - WF

Applying the ATM algorithm to the arc maps in Figure 4.3 produces the results in Figure 4.7.

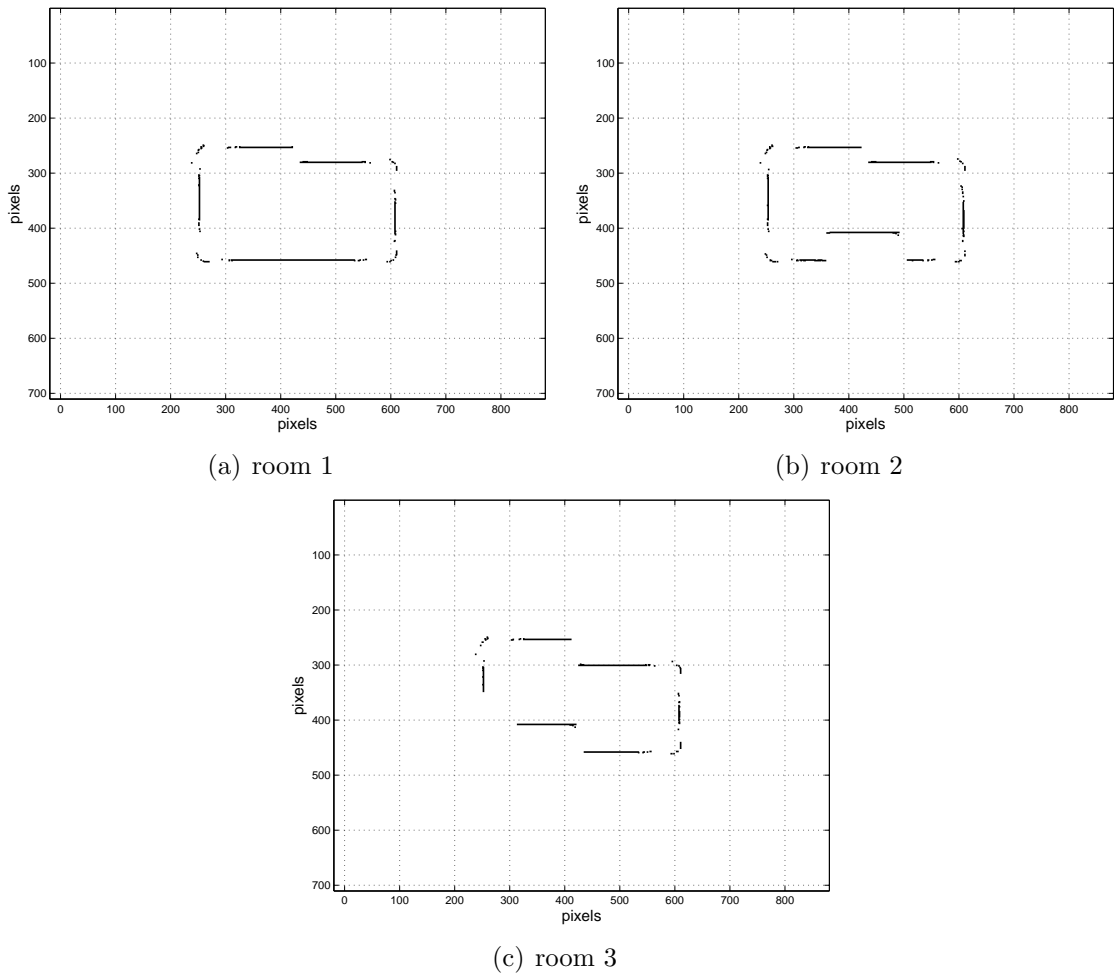


Figure 4.7: The result of applying the ATM algorithm to the arc maps obtained by WF in the three rooms.

As seen from the ATM results, this algorithm creates sparsely filled, yet accurate maps. Since the number of measurements for each implementation is kept constant, ATM is found to be requiring a higher number of measurements in order to have a more complete map. In all three of the rooms in Figure 4.7, there are many gaps in the surface profiles that ATM failed to fill. Corners are under-represented while the accuracy of the completed portion is satisfactory.

### Directional Maximum - WF

For a complete map-building application involving a motion-planning scheme such as wall following, the direction of the currently followed wall is the DOI. In other words, the DOI corresponds to the surface normal. In order to directionally process the maps in Figure 4.3, segmentation of the arc map into principal directional sub-maps is proposed. The segmentation is chosen to be in four principal directions in the Cartesian coordinate system. On the unit circle, the measurement directions are segmented into four groups according to their proximities to  $+\hat{x}$ ,  $+\hat{y}$ ,  $-\hat{x}$  and  $-\hat{y}$  axes, each measurement being assigned to the principal direction to which its transducer LOS is closest to. The arcs resulting from these grouped measurements form the sub-map segmentation of the complete arc map.

When the maps in Figure 4.3 are segmented into four principal directional sub-maps and directionally processed, the results shown in Figure 4.8 are obtained. No subsequent morphological processing is involved in this case. The resultant maps in Figure 4.8 are more populated than the previous ones, yet some of the artifacts were not cleaned properly.

In this section, we compared the five algorithms based on the maps constructed by the WF approach. The best results were obtained by BU and DM algorithms. In general, the arcs generated by reflections from corners seem to be generating a fair amount of the discontinuity observed in the arc maps, yet the processing methods seem to counter these effects considerably.

In the next section, we will make a comparison based on processed arc maps obtained when Voronoi diagram tracing is applied to the same three environments.

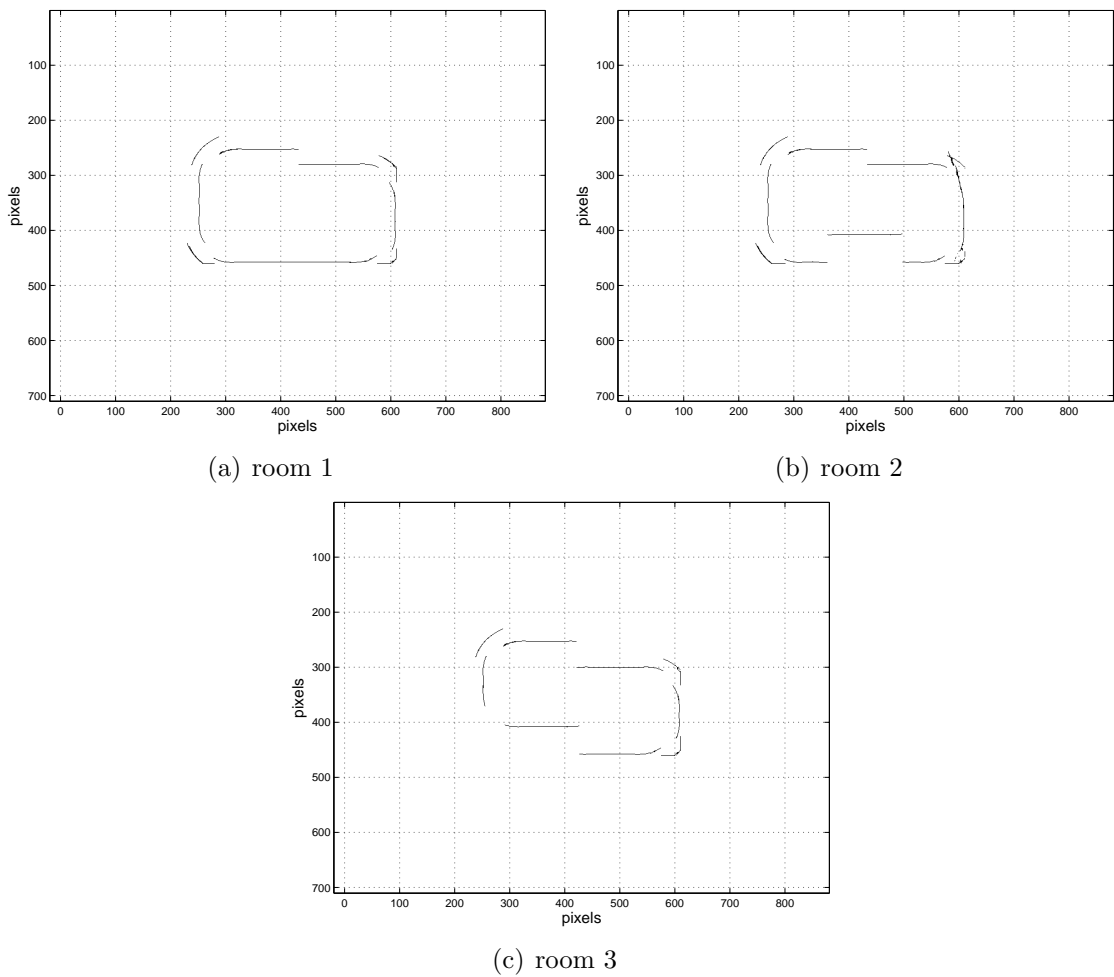


Figure 4.8: The result of applying DM to the arc maps obtained by WF in the three rooms.

## 4.2 Voronoi Diagram (VD) Tracing

On a 2-D map containing objects or obstacles, Voronoi diagram (VD) is a tool that can be used to obtain proximity information. When each point on the 2-D plane is assigned to the nearest obstacle/object, a number of points are bound to be left unassigned since they are equidistant to more than one point. These points, which are on equidistant lines to obstacles/objects form the VD. By constructing the VD of the unknown environment iteratively as described in [25, 26], and tracing the respective VD, structured motion planning can be achieved.

Although there exists iterative methods of VD construction for mobile robots that utilize the gradient-ascent operation to the minimum distance of a point to the set of all obstacles in the environment [25, 26], we employed a simpler approach for simulation purposes. The VDs utilized in our simulations are calculated with the knowledge of the room map in question. This way, the resultant VDs are ideal while iterative methodology requires high-level control rules to keep the robot close to the actual VD edges. One can employ the iterative approach in the real-life scenario, but the ideal VD is far better suited to our needs since the main scope of this thesis is not the motion-planning part of the application.

The VDs shown in Figure 4.9 are obtained from our room models given in Figure 4.1.

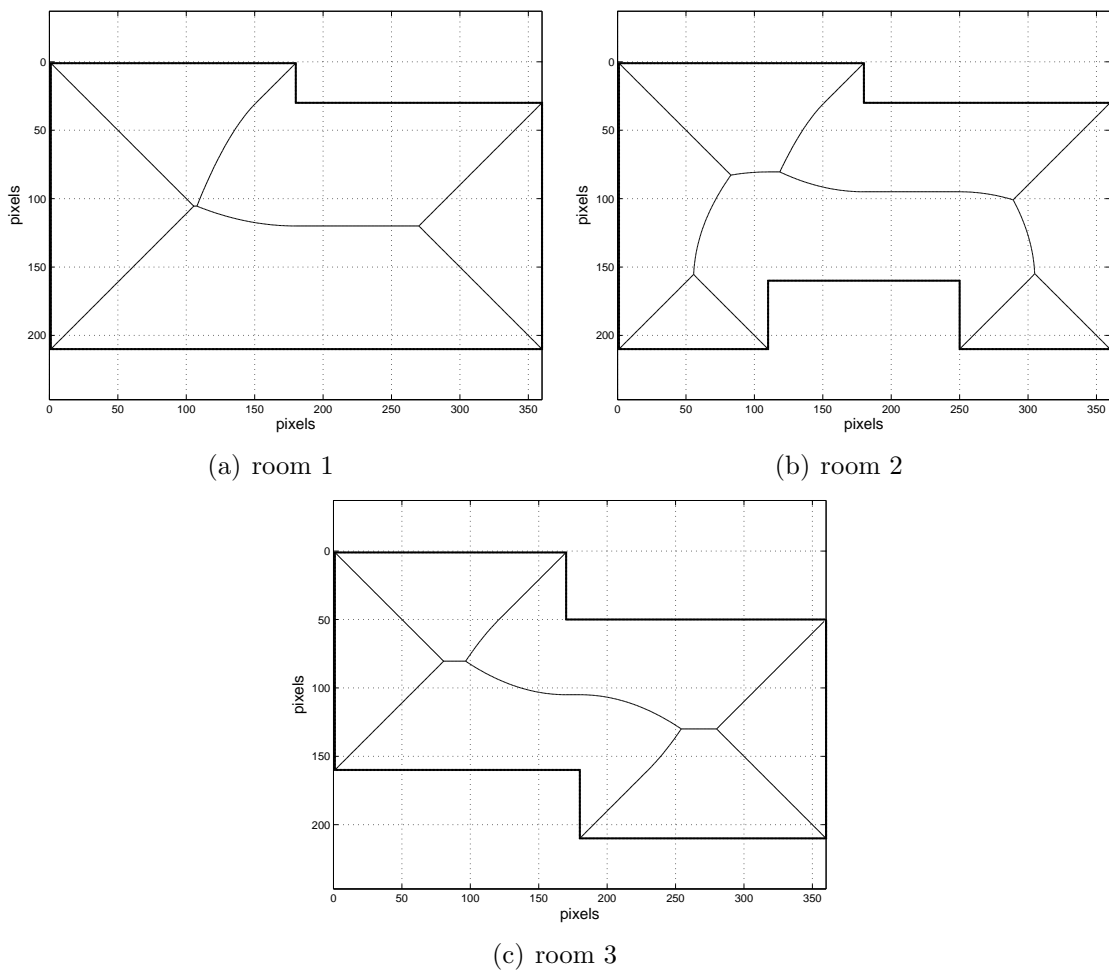


Figure 4.9: VDs of the three rooms.

When these VDs are sampled, i.e., a set of points along Voronoi edges are fetched, these points can be used as measurement points for map building. Downsampling these measurement points to a number comparable to that used in WF results at the decimated set of locations given in Figure 4.10. This is mainly done in order to make a fair comparison between WF and VD tracing cases and be able to operate in real-time. Hence, the resultant number of measurements is around 400 for each case.

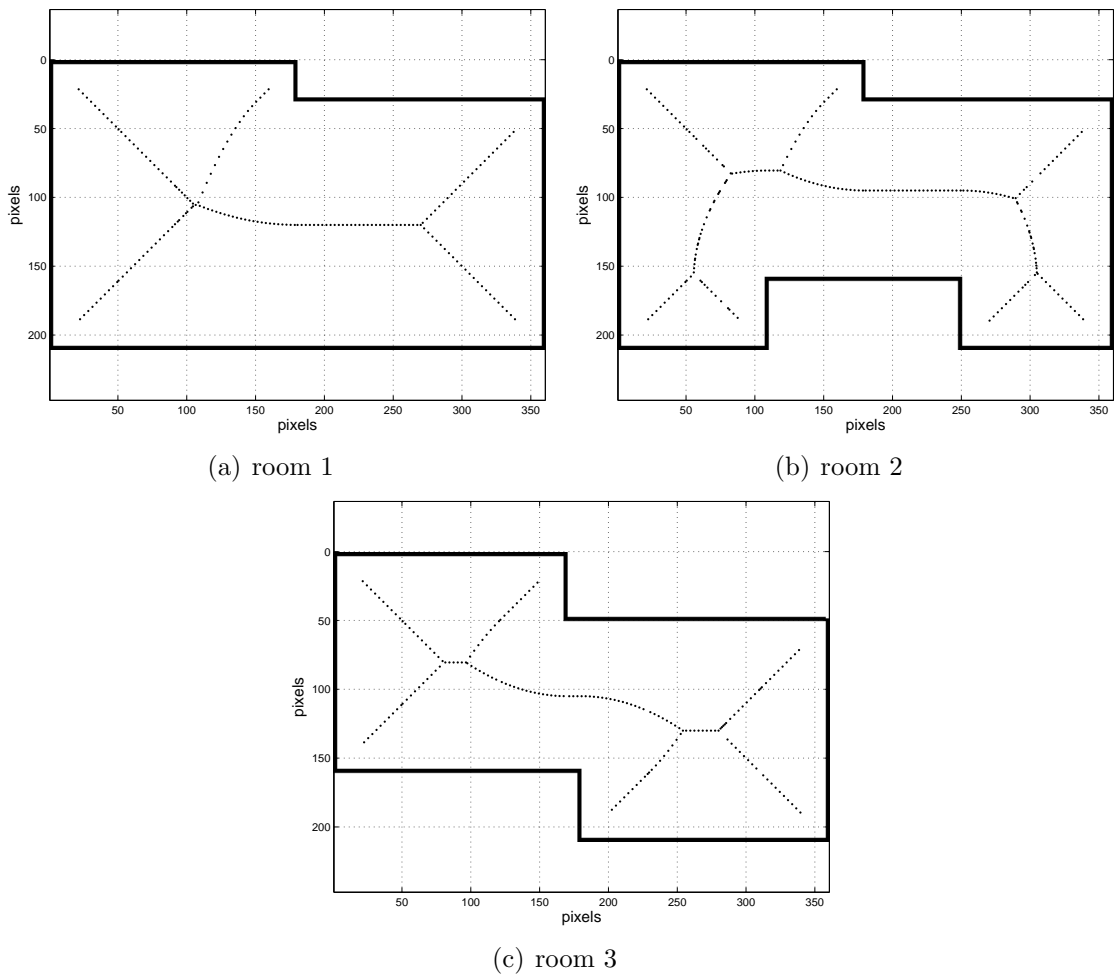


Figure 4.10: Sampled versions of the VDs indicating the points where measurements are taken.

Note that the VD samples that are too close to the corners (closer than 30 cm) have been removed since in real-life applications the mobile platform in use may not be able to get so close to corners due to its dimensions. As a result of collecting TOF data at the indicated positions and in multiple directions corresponding to the directions of the closest obstacles, arc maps in Figure 4.11 are obtained. These arc maps are processed with the same algorithms as before and the results are presented on the following pages.

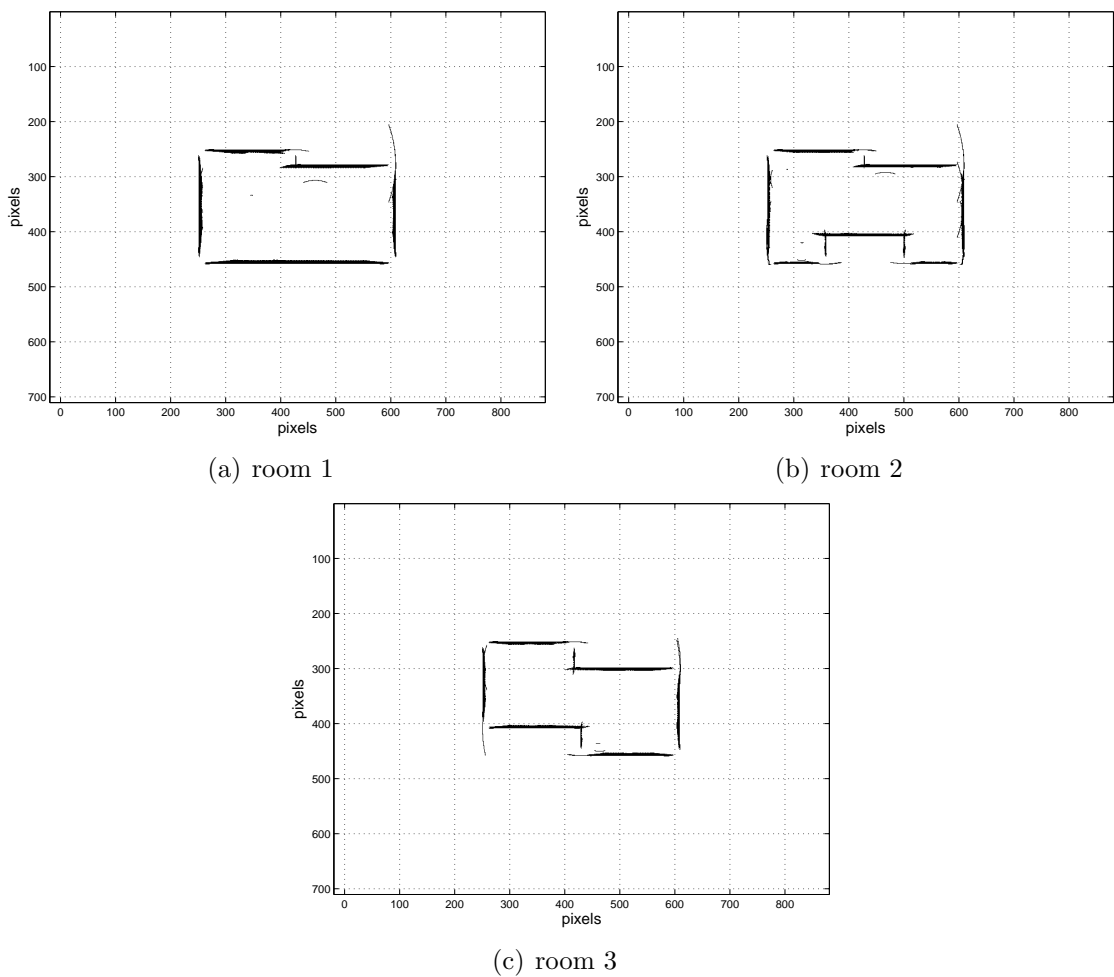


Figure 4.11: The arc maps obtained by VD tracing in the three rooms.

### Bayesian Update - VD Tracing

The results in Figure 4.12 are obtained by using the VD tracing measurement locations and the BU scheme. With VD tracing, BU gives fairly successful results



with minor gaps and some range uncertainty. Accurate planar profiles are obtained. Some corners are still incomplete due to the large ultrasonic beamwidth, yet most edges are well-defined.

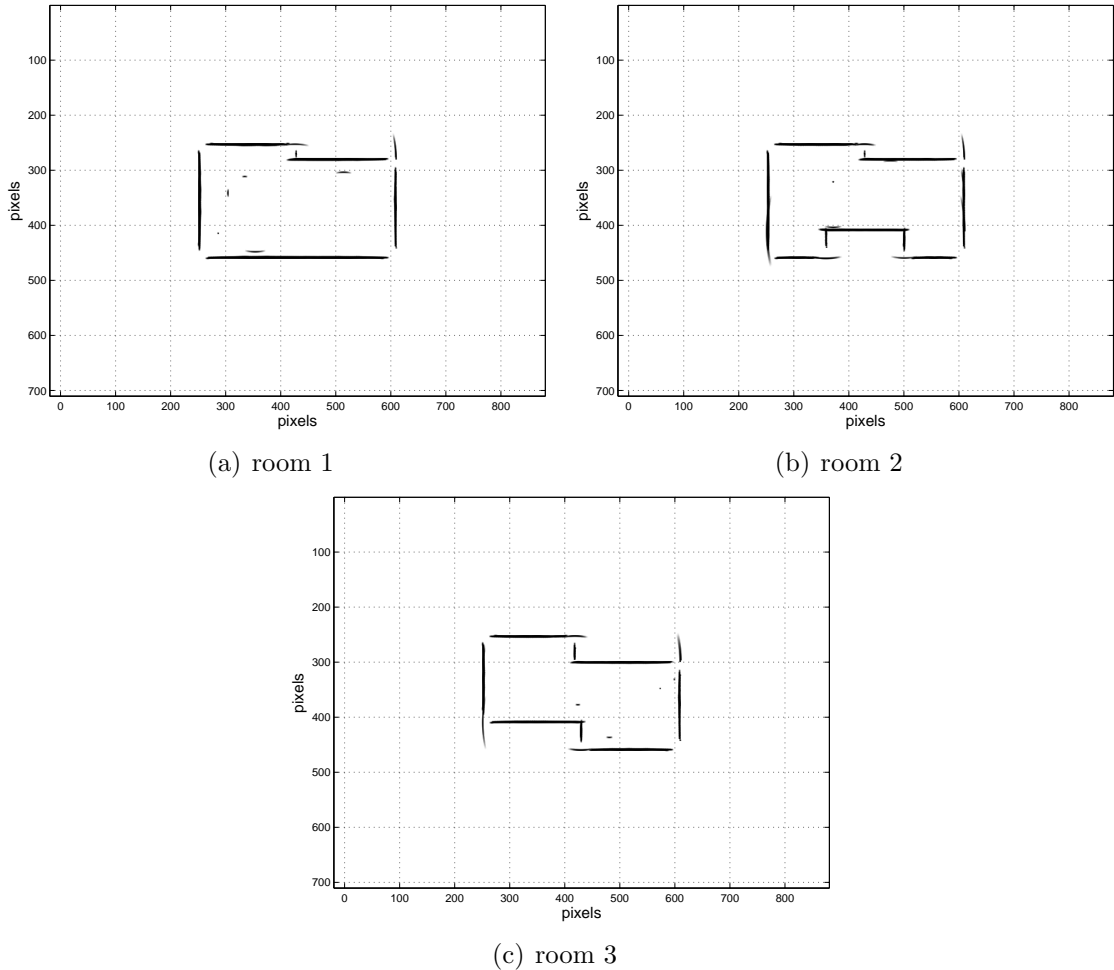


Figure 4.12: BU occupancy probability grids obtained by VD tracing in the three rooms.

### Morphological Processing - VD Tracing

After the arc maps in Figure 4.11 are processed using the thinning operation four times, the resultant maps in Figure 4.13 are obtained. As it was the case in WF, applying four repetitive thinning operations removes most of the artifacts but still leaves some defects on planar surfaces. This might be due to the large number of arcs that occupy the same area on the planar parts, but neither further nor less

thinning seems to be producing better results. Other morphological processes such as skeleton or erosion have also been tried but resulted in maps of lower quality.

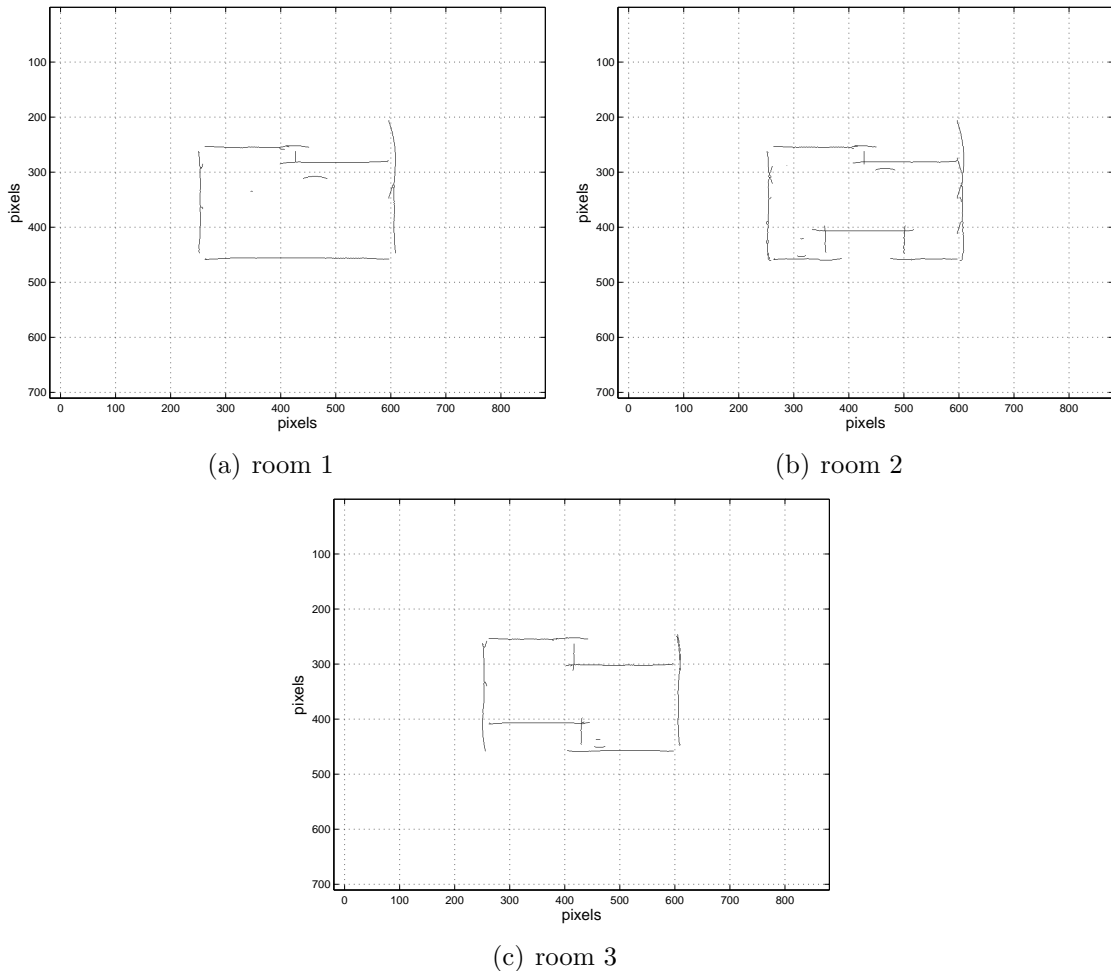


Figure 4.13: The result of applying MP to the arc maps obtained by VD tracing in the three rooms.

### Voting and Thresholding - VD Tracing

Voting and thresholding of the arc maps in Figure 4.11 with a threshold value of four resulted in the maps in Figure 4.14. Since planar parts have a higher density of intersecting arcs, cleaning those parts requires a threshold value larger than four, but higher thresholds clean the necessary features of the map such as corners and edges. Therefore, four is found to be the optimal threshold level for indoor simulation scenarios.

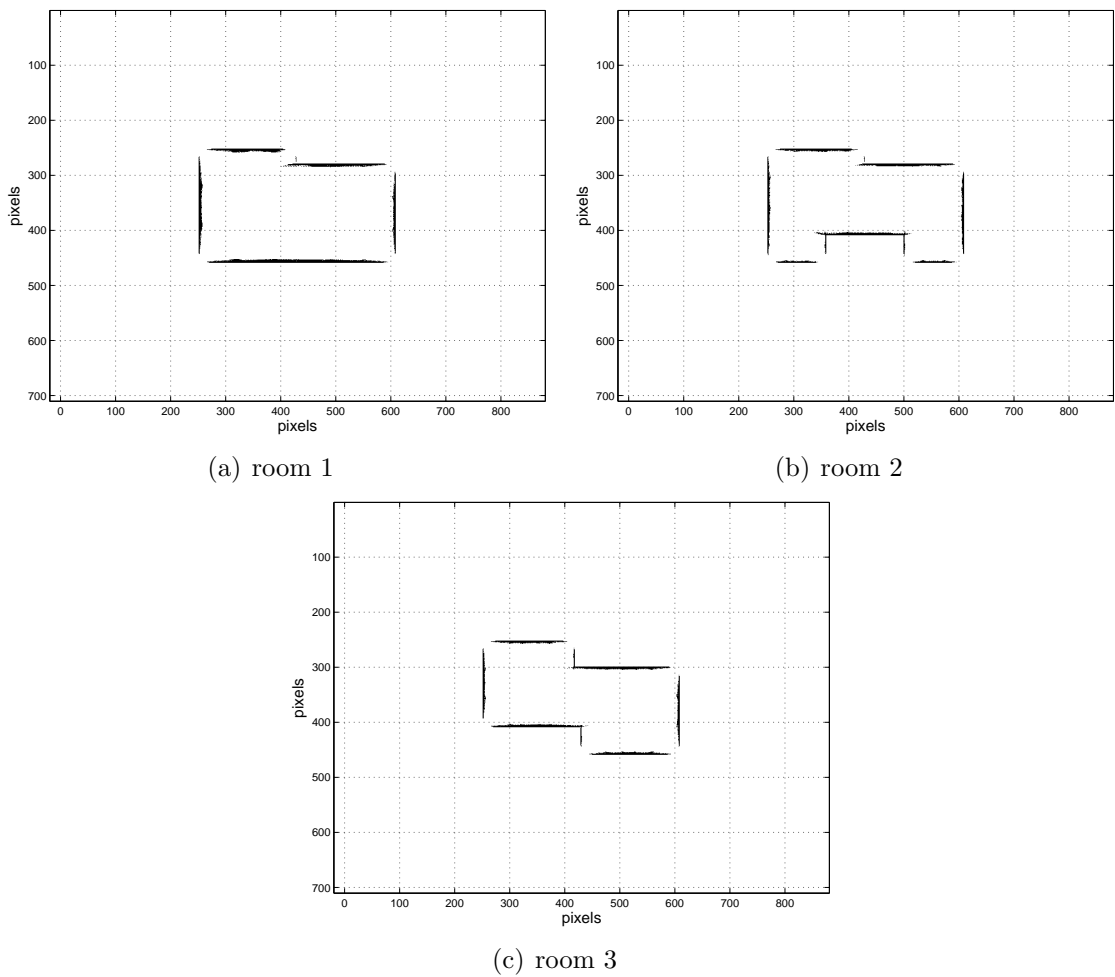


Figure 4.14: The result of applying VT to the arc maps obtained by VD tracing in the three rooms.

### Arc-Transversal Median - VD Tracing

Range measurements taken from VD tracing samples given in Figure 4.10 and applying the ATM algorithm produces the results in Figure 4.15.

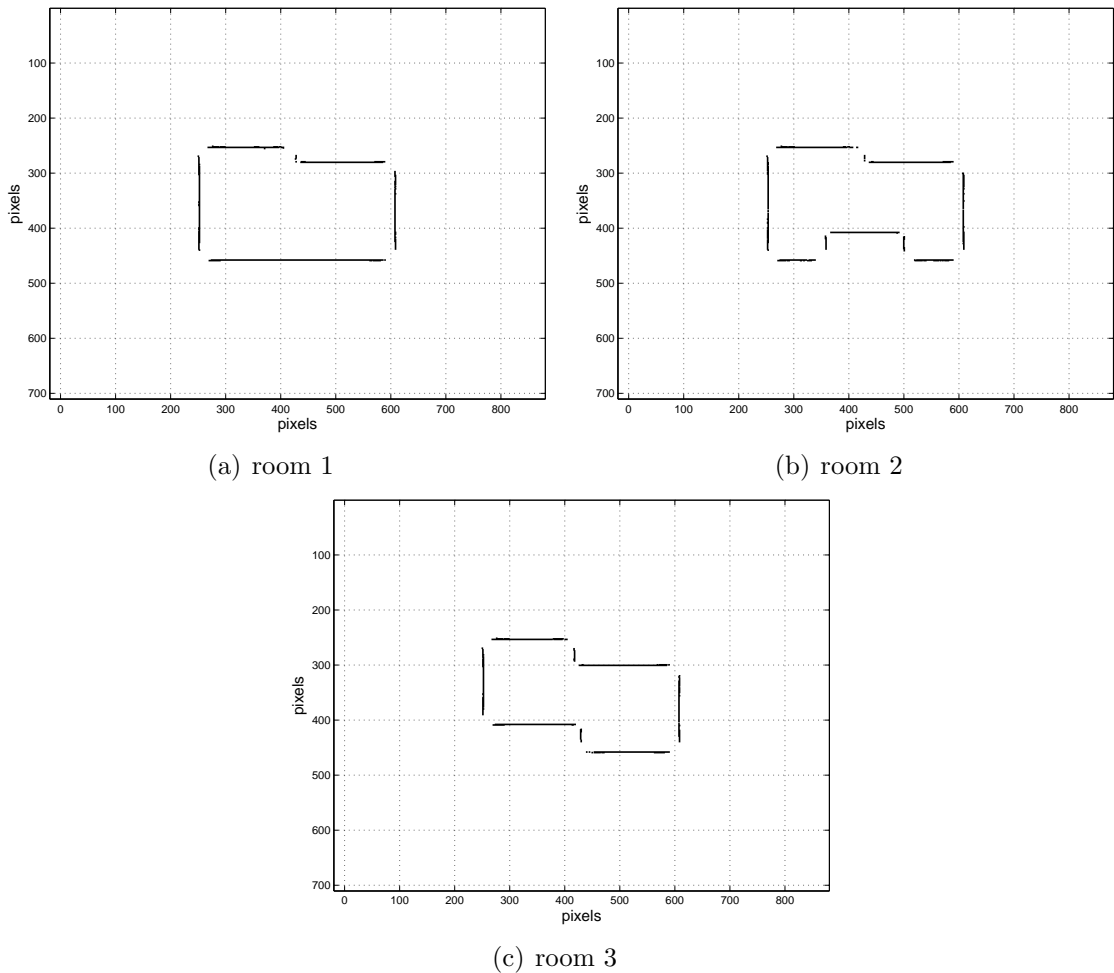


Figure 4.15: The result of applying the ATM algorithm to the arc maps obtained by VD tracing in the three rooms.

As in the WF scenario, the accuracy of the ATM algorithm is satisfactory while the resultant map is again more sparsely populated than the previous ones. The minor gaps in the planar surfaces and the missing corner and edge points indicates the necessity of a larger number of measurements to obtain a fully populated map with the ATM algorithm.

### Directional Maximum - VD Tracing

In this method, the arc maps in Figure 4.11 are segmented and directionally processed, to obtain the results in Figure 4.16. In VD tracing approach to motion planning, the DOI is the direction of the closest obstacle, similar to that being the direction of the followed wall in WF.

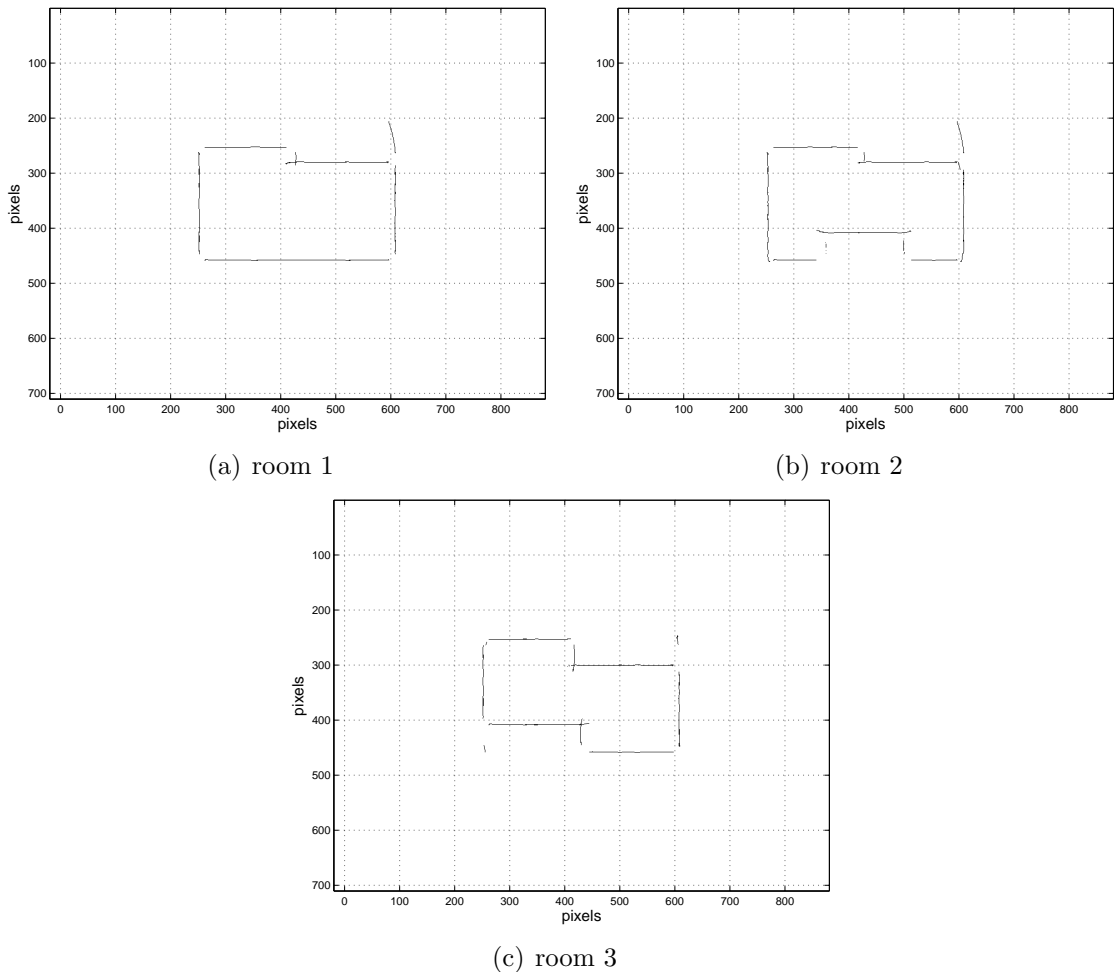


Figure 4.16: The result of applying DM to the arc maps obtained by VD tracing in the three rooms.

Some corner distortion is observable in the maps of each room in Figure 4.16. In all three maps, the upper righthand corner contains some uncleaned artifacts but the overall performance of DM in terms of artifact removal is satisfactory. The planar surfaces are observed to be represented with less range uncertainty than the other algorithms, which points to a higher accuracy.

### 4.3 Results of Indoor Mapping Simulations

For the indoor mapping scenarios, each simulation consists of approximately 400 TOF measurements comprising an arc map. The number of WF steps and the total number of points do change for each room type. Similarly, VD samples are bound to be in different numbers for each case. In indoor mapping scenarios, the algorithms compare as follows according to the error criteria described in Section 3.6. In Table 4.1, the mean absolute error for each of the three environments is given when motion planning is done by WF. Table 4.2 contains the fill ratios and Table 4.3 contains the processing times of the algorithms<sup>1</sup> for each room under the WF scheme. The best result of each column in the table is marked with bold faced fonts. When the two best results are comparable, both values are highlighted in the same way.

In terms of mean absolute error (Table 4.1), DM is superior to all algorithms. MP yields the best fill ratio (Table 4.2), however the results obtained by DM are comparable to those of MP. In terms of CPU time (Table 4.3) VT is the best, followed by DM and MP. ATM seems to require the largest CPU time and the lowest fill ratio for the given number of measurements.

	mean absolute error (pixels)		
method	room 1	room 2	room 3
BU	5.2	4.8	5.9
MP	7.8	9.1	7.0
VT	6.2	7.6	7.1
ATM	11.4	11.4	12.0
DM	<b>3.2</b>	<b>4.0</b>	<b>3.5</b>

Table 4.1: Mean absolute error – indoor simulations with WF.

---

<sup>1</sup>Internal MATLAB commands are used for time keeping, on a P4 3.06 MHz PC.

	fill ratio (percent)		
method	room 1	room 2	room 3
BU	89.8	91.8	83.0
MP	<b>96.7</b>	<b>96.1</b>	<b>90.5</b>
VT	85.7	88.5	80.9
ATM	63.7	63.6	57.2
DM	92.7	<b>94.4</b>	<b>88.5</b>

Table 4.2: Fill ratio – indoor simulations with WF.

	CPU time (sec)		
method	room 1	room 2	room 3
BU	6.2	9.0	5.6
MP	2.7	2.1	2.4
VT	<b>0.1</b>	<b>0.1</b>	<b>0.1</b>
ATM	941.2	3850.8	661.3
DM	1.7	1.8	1.9

Table 4.3: CPU time – indoor simulations with WF.

Tables 4.4–4.6 contain the error criteria for each room when motion planning is done by VD tracing.

	mean absolute error (pixels)		
method	room 1	room 2	room 3
BU	<b>4.7</b>	<b>4.8</b>	<b>4.4</b>
MP	6.1	7.2	6.8
VT	7.4	8.4	7.6
ATM	6.4	8.5	7.1
DM	<b>4.5</b>	<b>4.7</b>	5.3

Table 4.4: Mean absolute error – indoor simulations with VD tracing.

Referring to Table 4.4, DM is superior to the other algorithms in terms of mean absolute error but BU performs comparably according to this criteria. For fill ratios given in Table 4.5, MP and DM are the two best algorithms, closely followed by BU, but the overall performance of all algorithms with respect to fill ratio are comparable except that of ATM algorithm. In terms of CPU time tabulated in Table 4.6, VT is again superior, followed by DM and MP. The simplicity of the method results in far smaller computation times, while ATM, for instance, gives considerably larger processing costs due to the need to compute the intersection of arcs and the median of the intersections. ATM is also the algorithm resulting in the lowest fill ratios and

	fill ratio (percent)		
method	room 1	room 2	room 3
BU	<b>93.0</b>	94.6	<b>94.0</b>
MP	<b>93.2</b>	<b>97.1</b>	<b>95.0</b>
VT	91.4	90.7	89.8
ATM	74.2	71.5	72.7
DM	<b>93.4</b>	<b>96.7</b>	<b>93.7</b>

Table 4.5: Fill ratio – indoor simulations with VD tracing.

	CPU time (sec)		
method	room 1	room 2	room 3
BU	7.9	4.6	5.3
MP	2.2	2.6	2.7
VT	<b>0.1</b>	<b>0.1</b>	<b>0.1</b>
ATM	1206.7	898.3	597.0
DM	1.7	1.6	2.1

Table 4.6: CPU time – indoor simulations with VD tracing.

the largest CPU time. These results are quite consistent with those obtained from WF and the two simulation examples.

When Tables 4.1–4.6 are examined, the bold faced values that stand for the best values indicate that DM’s performance is satisfactory. Among the five approaches considered, it is the best algorithm in terms of mean absolute error and fill ratio, and second best to VT in processing cost. Its performance according to the fill ratio criterion is satisfactory, where it ranks between the best and the third best in different examples.

For a comparison between the motion-planning approaches (WF and VD tracing), VD tracing results in higher success measures. Generalized VD generation may be considered advantageous for map-building applications since it has a stronger promise of ground coverage and each 2-D environment is uniquely defined by its VD, however one has to consider the computational cost of VD tracing. Iterative building methods for the VD may be demanding for the mobile platform in use, hence the necessity to employ simpler and more cost-effective approaches such as WF.



In this chapter, we compared the algorithms for map-building in indoor environments using two ways of motion planning. In the final chapter we discuss the main conclusions and future extensions of the work reported here.

# Chapter 5

## Conclusions

The main contribution of this thesis has been providing a comparison between different algorithms for processing ultrasonic arc maps for map-building purposes. The results indicate that the newly proposed DM algorithm has some advantages over the existing algorithms, while among the existing four algorithms each has stronger or weaker characteristics that might be suitable for certain situations or conditions. Having the minimum mean absolute error, DM should be considered a good choice in most cases, while strict requirements on computational cost might lead to the use of VT algorithm since it requires far smaller CPU time to operate. In addition, MP might be considered when a rough yet full view of the environment is required as the computational cost of MP is still achievable in real-time even though the associated mean absolute errors are not as good as those of DM.

DM in itself has added an important aspect to the map-building algorithms which is the direction of interest. The sense of direction readily available in most motion-planning schemes is shown to be an effective addition when incorporated into the map-building algorithm. The directional awareness of the mobile platform for the sake of surface or profile extraction was proved to deliver satisfactory maps.

In addition, the compared motion-planning approaches showed that VD tracing is more successful in ground coverage since it includes a more systematic and complete approach to the entire environment. WF also has its merits as the iterative

methods to generate a WF motion-plan is far simpler than that of VD tracing and in most artificial environments simple rule-based algorithms perform well for WF. VD tracing seems to be the better choice if the computational cost is of secondary importance as it might be computationally demanding for complex environments.

As for future extensions, multiple reflections might be included in the simulated signal model. Iterative methods for VD generation would also be a good capability for the mobile platform since a priori knowledge of the VD might not be readily available. A more complex WF algorithm can be included in order to map arbitrarily curved surfaces that can be encountered in natural environments. For DM, a self-centered polar processing scheme can be developed where several separate locations of the mobile platform in the environment might be chosen and used as central points from which the arc map can be radially processed and then fused. Multiple maxima along directional array can be handled according to the general curvature of the arcs intersecting at each pixel. Applying active contour models used in image processing and known as “snakes” to the resultant maps might improve the fill ratios. The results might be verified experimentally and the approaches can be extended to other sensing modalities.

# Appendix A

## Ultrasonic Signal Models

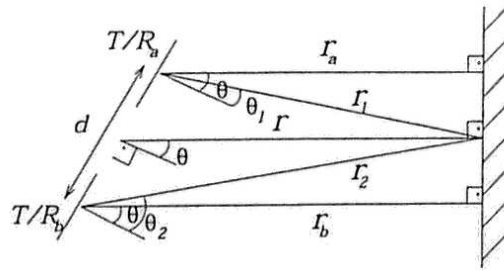


Figure A.1: Geometry of the problem with the given sensor pair when the target is a plane (adopted from [1]).

The echo models used in this thesis and presented in Chapter 2 are based on [1]. For a planar target and separate transducers working as transmitter and receiver (transducer  $a$  and  $b$ ), the geometry of reflection is illustrated in Figure A.1. Since each transducer can be employed both as a transmitter and receiver, a set of four TOF measurements are obtained when the transducers are fired in sequence. From the geometry, the TOF measurements for each transmitter and receiver pair are found as

$$\begin{aligned}
t_{aa} &= \frac{2r_a}{c}, \\
t_{ab} &= t_{ba} = \frac{r_1 + r_2}{c}, \\
t_{bb} &= \frac{2r_b}{c},
\end{aligned}$$

where  $t_{ab}$  denotes TOF extracted from  $A_{ab}(r, \theta, d, t)$  which is the echo signal transmitted by  $a$  and received by  $b$  at time  $t$ . The detected signals by each transmitter and receiver can be modeled as:

$$\begin{aligned}
A_{aa}(r, \theta, d, t) &= A_{max} \frac{r_{min}}{r_a} e^{-\frac{\theta^2}{2\sigma_T^2}} e^{-\frac{(t-t_{aa}-t_d)^2}{2\sigma^2}} \sin[2\pi f_0(t - t_{aa})] \\
A_{ab}(r, \theta, d, t) &= A_{max} \frac{2r_{min}}{r_1 + r_2} e^{-\frac{\theta_1^2 + \theta_2^2}{2\sigma_T^2}} e^{-\frac{(t-t_{ab}-t_d)^2}{2\sigma^2}} \sin[2\pi f_0(t - t_{ab})] \\
A_{ba}(r, \theta, d, t) &= A_{max} \frac{2r_{min}}{r_1 + r_2} e^{-\frac{\theta_1^2 + \theta_2^2}{2\sigma_T^2}} e^{-\frac{(t-t_{ba}-t_d)^2}{2\sigma^2}} \sin[2\pi f_0(t - t_{ba})] \\
A_{bb}(r, \theta, d, t) &= A_{max} \frac{r_{min}}{r_b} e^{-\frac{\theta^2}{2\sigma_T^2}} e^{-\frac{(t-t_{bb}-t_d)^2}{2\sigma^2}} \sin[2\pi f_0(t - t_{bb})]
\end{aligned}$$

In all of the signal models,  $\sigma_T = \frac{\theta_0}{2}$ ,  $t_d = \frac{3}{f_0}$ ,  $\sigma = 0.001$  sec,  $f_0 = 49.4$  kHz, and  $r_{min} = 5.7$  cm. The form of the range attenuation term  $r_1 + r_2$  in  $A_{ab}(r, \theta, d, t)$  and  $A_{ba}(r, \theta, d, t)$  is due to specular reflection of the beam.

# Appendix B

## Wall-following (WF) Algorithm

The WF algorithm employed in our simulations is a relatively simple and rule-based approach similar to that described in [46]. If the bearing of the mobile robot is taken as the reference frame on the 2-D plane, the general intention of the robot is to keep the wall to be followed on  $+\hat{y}$  direction at all times. This is done as follows:

1. Initialization step: The robot is at an unknown, arbitrary location. Sixteen range measurements in sixteen directions from the initial point, uniformly distributed on the unit circle with  $22.5^\circ$  intervals are obtained. The minimum value among these range measurements, which corresponds to the closest obstacle, is taken as the direction of the surface/wall to be followed.
2. First step: The robot approaches to or goes away from the closest surface until the distance to the surface is 60 cm. Then the robot performs a  $-90^\circ$  rotation in order to align the wall to  $+\hat{y}$  direction of its internal frame of reference.
3. Step number 2 to  $N$ : Until the robot is in proximity of the initial point (at 20 cm distance to the starting location) or the predetermined number of steps (an upper limit of 100 steps are chosen) are complete, the robot repeats this procedure:

Take two range measurements.  $r_1$  being the range measured directly ahead or in  $+\hat{x}$  direction in robot's reference frame and  $r_2$  being the range measured in

$+\hat{y}$  direction in robot's reference frame, check for the following:

- (a) if  $r_2 > 80$  cm, then the followed wall is lost. Perform a  $+90^\circ$  turn and move 60 cm in three separate steps of 20 cm each.
- (b) if  $r_2 \leq 80$  cm and  $r_1 > 60$  cm, then take a step ahead. Move 15 cm ahead and make any additional course correction necessary to keep the distance to the wall ( $r_2$ ) at 60 cm.
- (c) if both  $r_2 \leq 80$  cm and  $r_1 \leq 60$  cm, then perform a  $-90^\circ$  turn. This corresponds to the presence of a left-hand corner, so the new wall is followed after this step.

The above described procedure is found to be simple enough yet effective in most indoor environments that have artificial surfaces and obstacles, interfacing at right angles. A flow chart of the algorithm can be found in Figure B.1. The threshold values for  $r_1$  and  $r_2$  are set after a number of trials. The result of this algorithm when applied to the room examples of Figure 4.1 in Chapter 4 are presented in Figure 4.2.

For more complex environments and/or cases where computational cost of the algorithm is not an issue, potential-based WF algorithms can also be employed [19–21].

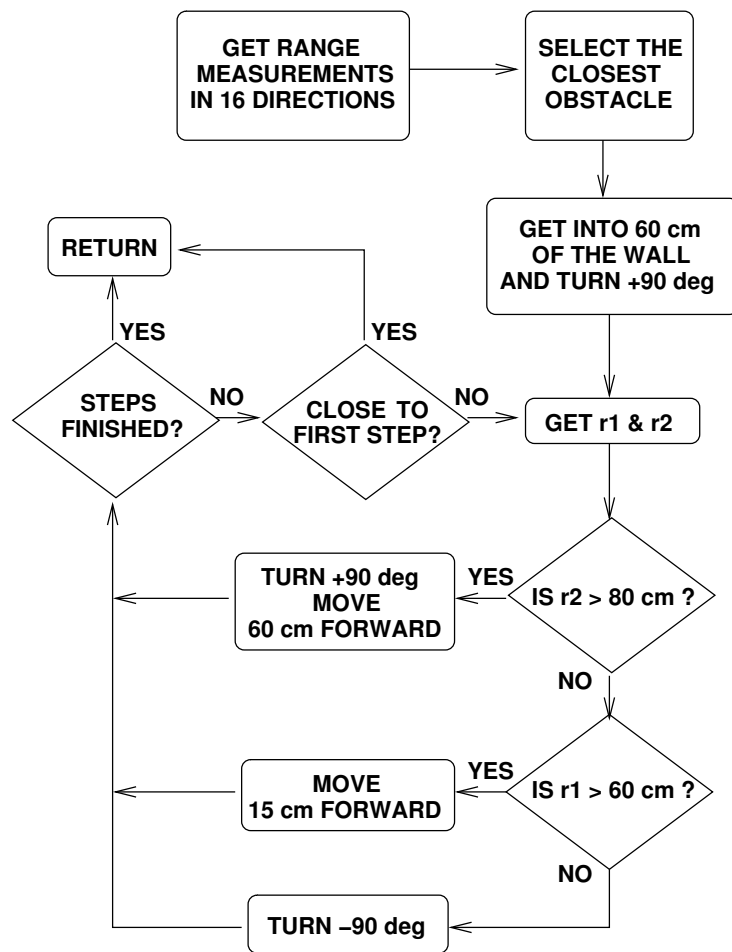


Figure B.1: WF algorithm flowchart.



# Appendix C

## MATLAB Simulation Codes

The MATLAB code used in the simulations can be found on the following pages.

```

function wall_foll_map(type)

% WALL FOLLOWING TYPE MOTION-PLANNING BASED
% MAP BUILDING SCRIPT, UTILIZING MP, VT, ATM & DM
% GETS THE PARAMETER type TO INDICATE ROOM TYPE

disp('=====')
disp(['Wall Following, Room Type ' int2str(type)])
disp('=====')

room=draw_room4(type);
print('-deps',strcat('room_def_type_',int2str(type)))
[Y,X]=size(room);
% DEFINE THE ROOM, EXPORT EPS FIGURE OF THE ROOM AND GET SIZE

load(strcat('wall_foll_type_',int2str(type)));
% LOAD WALL FOLLOWING STEP LOCATIONS

%=====
% MORPHOLOGICAL PROCESSING
%=====
x_array1=wf(1,:);
y_array1=wf(2,:);
b_array1=wf(3,)+90;
% EXTRACT LOCATIONS AND BEARINGS

x_array=interp(x_array1,10);
y_array=interp(y_array1,10);
b_array=interp(b_array1,10);
% INTERPOLATE STEP POSITIONS TO GET MEASUREMENT LOCATIONS

x_array=fix(x_array);
y_array=fix(y_array);
b_array=fix(b_array);
totalsonarno=length(x_array)
% FIX THE PIXELS TO SMALLEST INTEGER AND DISPLAY TOTAL MEASUREMENT POINT #

base_dm=zeros(Y+500,X+500);
% ALLOCATE EMPTY ARC-MAP ARRAY FOR BOOK KEEPING

for son=1:length(x_array)
    base_dm=sonarPut5(x_array(son),y_array(son),b_array(son),room,base_dm);
end
% PLACE THE SONARS

base=base_dm;
% COPY THE ARC MAP TO BE PROCESSED

tic
% START KEEPING THE TIME

base2=logical(sign(base));

```

```

% CONVERT ARC MAP TO LOGICAL

base3=bwmorph(base2,'thin',4);
% APPLY MORPHOLOGICAL PROCESSING

time_morph=toc
% GET THE COMPUTATION TIME

figure
colormap(gray(2))
image(2-2*base2)
grid on
xlabel('pixels','FontSize',14)
ylabel('pixels','FontSize',14)
axis equal
print('-deps',strcat('mpl_wf_type_',int2str(type)))
% DISPLAY AND EXPORT BINARY ARC MAP

figure
colormap(gray(2))
image(2-2*base3)
grid on
xlabel('pixels','FontSize',14)
ylabel('pixels','FontSize',14)
axis equal
print('-deps',strcat('mp2_wf_type_',int2str(type)))
% DISPLAY AND EXPORT MP ARCS

%=====
% VOTING AND THRESHOLDING
%=====
tic
% START KEEPING THE TIME

thres=4;
% SET THE THRESHOLD

base4=sign(floor(base/thres));
% APPLY THE THRESHOLD

time_vote=toc
% GET THE COMPUTATION TIME

figure
colormap(gray(255))
scale=255/max(max(base));
image(255-scale*base)
axis equal
grid on
xlabel('pixels','FontSize',14)
ylabel('pixels','FontSize',14)
print('-deps',strcat('vt1_wf_type_',int2str(type)))

```

```

% DISPLAY AND EXPORT INTEGER ARC MAP

figure
colormap(gray(255))
image(255-255*base4)
grid on
xlabel('pixels','FontSize',14)
ylabel('pixels','FontSize',14)
axis equal
print('-deps',strcat('vt2_wf_type_',int2str(type)))
% DISPLAY AND EXPORT VT ARC MAP

%=====
% ATM
%=====
arcs=0;
% ALLOCATE EMPTY ARRAY FOR ARC PIXEL LOCATIONS

tim_atm=0;
% RESET TIME KEEPING VARIABLE

for son=1:length(x_array)
    arcs=sonarATM2(x_array(son),y_array(son),b_array(son),room,arcs,son,tim_atm);
end
% GET THE ARC PIXEL LOCATIONS

tic
% START KEEPING THE TIME

[arcNo,abc,acb]=size(arcs);
arcLength=length(arcs(1,:));
% GET ALL SIZES OF THE ARC PIXEL LOCATION ARRAY

for arc=1:arcNo
    il=1;
    if (arcs(arc,1)~=0) || (arcs(arc,1,2)~=0)

        for pix=1:arcLength
            if (arcs(arc,pix,1)~=0) || (arcs(arc,pix,2)~=0)
                xx=arcs(arc,pix,1);
                yy=arcs(arc,pix,2);
                for sc1=1:arcNo
                    for sc2=1:arcLength
                        if (arcs(sc1,sc2,1)==xx) && (arcs(sc1,sc2,2)==yy)
                            if (sc1==arc) || (sc2==pix)
                                arcs2(arc,il,1)=xx;
                                arcs2(arc,il,2)=yy;
                                il=il+1;
                            end
                        end
                    end
                end
            end
        end
    end
end
end

```

```

end
end
end
% COMPUTE THE INTERSECTIONS OF THE ARCS

base_atm=zeros(Y+500,X+500);
% ALLOCATE ATM BASE FOR WORLD MODEL

[mini,1]=min(arcs2(:,1),[],2);
for arc=1:arcNo
    if i(arc)~=1
        x_cor(arc)=fix(median(arcs2(arc,1:(i(arc)-1),1)));
        y_cor(arc)=fix(median(arcs2(arc,1:(i(arc)-1),2)));
    end
end
% COMPUTE THE MEDIAN OF INTERSECTIONS

for pix=1:length(x_cor)
    if x_cor(pix)~=0
        base_atm(y_cor(pix),x_cor(pix))=1;
    end
end
% PLACE THE INTERSECTIONS ON THE BASE

time_atm=toc
% GET THE COMPUTATION TIME

base_atm=double(bwmorph(base_atm,'dilate'));
% DILATE THE ATM MAP FOR BETTER DISPLAY

figure
colormap(gray(255))
image(255-255*sign(base_atm))
axis equal
grid on
xlabel('pixels','FontSize',14)
ylabel('pixels','FontSize',14)
print('-deps',strcat('atm_wf_type_',int2str(type)))
% DISPLAY AND EXPORT THE ATM MAP

%=====
% DIRECTIONAL MAXIMUM
%=====
figure
colormap(gray(255))
image(255-255*sign(base_dm))
axis equal
grid on
xlabel('pixels','FontSize',14)
ylabel('pixels','FontSize',14)

```

```

print('-deps',strcat('dm1_wf_type_',int2str(type)))
% DISPLAY AND EXPORT INTEGER ARC MAP

b1i=1;
b2i=1;
b3i=1;
b4i=1;
% SET THE COUNTERS

for son=1:length(x_array)
    switch floor(mod(b_array(son)+45),360)/90
        case 0
            x_array_1(b1i)=x_array(son);
            y_array_1(b1i)=y_array(son);
            b_array_1(b1i)=b_array(son);
            b1i=b1i+1;
        case 1
            x_array_2(b2i)=x_array(son);
            y_array_2(b2i)=y_array(son);
            b_array_2(b2i)=b_array(son);
            b2i=b2i+1;
        case 2
            x_array_3(b3i)=x_array(son);
            y_array_3(b3i)=y_array(son);
            b_array_3(b3i)=b_array(son);
            b3i=b3i+1;
        case 3
            x_array_4(b4i)=x_array(son);
            y_array_4(b4i)=y_array(son);
            b_array_4(b4i)=b_array(son);
            b4i=b4i+1;
        case 4
            x_array_4(b4i)=x_array(son);
            y_array_4(b4i)=y_array(son);
            b_array_4(b4i)=b_array(son);
            b4i=b4i+1;
    end
end
% SEGMENT THE MEASUREMENTS ACCORDING TO THEIR DIRECTIONS

base_dm1=zeros(Y+500,X+500);
base_dm2=zeros(Y+500,X+500);
base_dm3=zeros(Y+500,X+500);
base_dm4=zeros(Y+500,X+500);
% FORM FIVE SEPARATE ARC MAP BASIS

for son=1:length(x_array_1)
    base_dm1=sonarPut5(x_array_1(son),y_array_1(son),b_array_1(son),room,base_dm1);

```

```

end

for son=1:length(x_array_2)
    base_dm2=sonarPut5(x_array_2(son),y_array_2(son),b_array_2(son),room,base_dm2);
end

for son=1:length(x_array_3)
    base_dm3=sonarPut5(x_array_3(son),y_array_3(son),b_array_3(son),room,base_dm3);
end

for son=1:length(x_array_4)
    base_dm4=sonarPut5(x_array_4(son),y_array_4(son),b_array_4(son),room,base_dm4);
end
% PLACE THE SONAR MEASUREMENTS

tic
% START KEEPING THE TIME
base_dm1a=maxdisp_dir(base_dm1,0);
base_dm2a=maxdisp_dir(base_dm2,90);
base_dm3a=maxdisp_dir(base_dm3,0);
base_dm4a=maxdisp_dir(base_dm4,90);
% DM PROCESS THE SEGMENTED MAPS

base_dm_f=base_dm1a+base_dm2a+base_dm3a+base_dm4a;
% SUPERPOSE THE SEGMENTS

tim_dm=toc
% GET THE COMPUTATION TIME

figure
colormap(gray(255))
image(255-255*sign(base_dm_f))
axis equal
grid on
xlabel('pixels','FontSize',14)
ylabel('pixels','FontSize',14)
print('-deps',strcat('dm4_wf_type_',int2str(type)))
% DISPLAY AND EXPORT DM ARC MAP

room=draw_room3(type);
% CREATE TRUE ROOM FOR BENCHMARKING

[s1,s2]=room_suc(type,room,base3,base4,base_atm,base_dm_f);
% GET THE SUCCESS MEASURES

%=====
%=====

function wall_foll_b_map(type)
% WALL FOLLOWING TYPE MOTION-PLANNING BASED

```

```

% MAP BUILDING SCRIPT, UTILIZING BU
% GET THE PARAMETER type TO INDICATE ROOM TYPE

disp('=====')
disp(['Wall Following, Room Type ' int2str(type)])
disp('=====')

room=draw_room4(type);
[Y,X]=size(room);
% DEFINE THE ROOM AND GET SIZE

base=zeros(Y+500,X+500);
% ALLOCATE EMPTY ARC-MAP ARRAY FOR BOOK KEEPING

load(strcat('wall_foll_type_',int2str(type)));
% LOAD WALL FOLLOWING STEP POSITIONS

x_array1=wf(1,:);
y_array1=wf(2,:);
b_array1=wf(3,:)+90;
% EXTRACT THE POSITIONS

x_array=interp(x_array1,10);
y_array=interp(y_array1,10);
b_array=interp(b_array1,10);
% INTERPOLATE TO MEASUREMENT POSITIONS

x_array=fix(x_array);
y_array=fix(y_array);
b_array=mod(fix(b_array),360);
% FIX THE POSITIONS TO SMALLEST INTEGER
totalsonarno=length(x_array)
% DISPLAY TOTAL MEASUREMENT POINT #

for son=1:length(x_array)
    [x_list,y_list,b_list,d_list]=sonarPut5_d(x_array(son),y_array(son),b_array(son),room,base);
    x_array1(son^4-3:son^4)=x_list;
    y_array1(son^4-3:son^4)=y_list;
    b_array1(son^4-3:son^4)=b_list;
    d_array1(son^4-3:son^4)=d_list;
end
% GET THE MEASUREMENTS

x_array=x_array1;
y_array=y_array1;
b_array=b_array1;
d_array=d_array1*100;
% COPY THE MEASUREMENTS TO BE PROCESSED

epsi=2;
R_min=5.7;

```

```

omega=25;
empty_array=zeros(Y+500,X+500);
occupied_array=zeros(Y+500,X+500);
% SET PARAMETERS AND ALLOCATE PROBABILITY DENSITY ARRAYS

tic
% START KEEPING THE TIME

for son=1:length(x_array)
    R=d_array(son);
    if R=0;
        xs=x_array(son);
        ys=y_array(son);
        bs=b_array(son);

        x_lim1=fix(min([(x_array(son)+d_array(son)*cosd(b_array(son)+omega/2),x_array(son)+d_array(son)*cosd(b_array(son)-omega/2),x_array(son)+d_array(son)*cosd(b_array(son))])));
        x_lim2=fix(max([(x_array(son)+d_array(son)*cosd(b_array(son)+omega/2),x_array(son)+d_array(son)*cosd(b_array(son)-omega/2),x_array(son)+d_array(son)*cosd(b_array(son)))]));
        y_lim1=fix(min([(y_array(son)-d_array(son)*sind(b_array(son)+omega/2),y_array(son)-d_array(son)*sind(b_array(son)-omega/2),y_array(son)-d_array(son)*sind(b_array(son)))]));
        y_lim2=fix(max([(y_array(son)-d_array(son)*sind(b_array(son)+omega/2),y_array(son)-d_array(son)*sind(b_array(son)-omega/2),y_array(son)-d_array(son)*sind(b_array(son)))]));

        for x=x_lim1:x_lim2
            for y=y_lim1:y_lim2

                sig=sqrt((x-xs)^2+(y-ys)^2);
                thet=atan2((y-ys),(x-x));
                thet=(180*(thet+pi)/pi-bs);

                if abs(thet)<=omega/2
                    E_a=1-(2*thet/omega)^2;
                else
                    E_a=0;
                end

                if sig <= (R-epsi)
                    E_r=1-((sig)/(R-epsi))^2;
                else
                    E_r=0;
                end

                if abs(R-sig)<=epsi
                    O_r=1-((sig-R)/epsi)^2;
                else
                    O_r=0;
                end
            end
        end
    end
end

```

```

end

p_E=E_r*E_a;
p_O=O_r*E_a;

empty_array(y+250,x+250)=empty_array(y+250,x+250)+p_E*empty_array(y+250, x
x+250)*p_E;
occupied_array(y+250,x+250)=occupied_array(y+250,x+250)+p_O*occupied_array(x
(y+250,x+250)*p_O;

end
end
end
end
% UPDATE THE PROBABILITY DENSITY ARRAYS FOR EACH MEASUREMENT

time_bayes=toc
% GET THE COMPUTATION TIME

figure
colormap(gray(255))
image(255-255*empty_array)
axis equal
grid on
xlabel('pixels','FontSize',14)
ylabel('pixels','FontSize',14)
print('-deps',strcat('bayes_e_wf_type_',int2str(type)))
% DISPLAY AND EXPORT EMPPTINESS PROBABILITIES

figure
colormap(gray(255))
image(255-255*occupied_array)
axis equal
grid on
xlabel('pixels','FontSize',14)
ylabel('pixels','FontSize',14)
print('-deps',strcat('bayes_wf_type_',int2str(type)))
% DISPLAY AND EXPORT OCCUPANCY PROBABILITIES

by_rm=occupied_array(251:460,251:610);
tip=type;
rm=room;
switch tip
case {1}
alt_rm=rm(151:210,3:357);
alt_by=by_rm(151:210,3:357);

ust_rm=rm(1:60,3:357);
ust_by=by_rm(1:60,3:357);

sol_rm=rm(3:207,1:60);
sol_by=by_rm(3:207,1:60);

```

```

sag_rm=rm(33:207,301:360);
sag_by=by_rm(33:207,301:360);

case {2}
alt_rm=rm(151:210,3:357);
alt_by=by_rm(151:210,3:357);

ust_rm=rm(1:60,3:357);
ust_by=by_rm(1:60,3:357);

sol_rm=rm(3:207,1:60);
sol_by=by_rm(3:207,1:60);

sag_rm=rm(33:207,301:360);
sag_by=by_rm(33:207,301:360);

case {3}
alt_rm=rm(151:210,3:357);
alt_by=by_rm(151:210,3:357);

ust_rm=rm(1:60,3:357);
ust_by=by_rm(1:60,3:357);

sol_rm=rm(3:157,1:60);
sol_by=by_rm(3:157,1:60);

sag_rm=rm(53:207,301:360);
sag_by=by_rm(53:207,301:360);

end

rml=[sag_rm sol_rm ust_rm alt_rm];
byl=[sag_by sol_by ust_by alt_by];
% EXPORT AND SHAPE THE ARC MAP FOR SUCCESS MEASURE COMPUTATION

[Y,max_rm]=max(rml);
[Y,max_by]=max(byl);

disp(['Mean Absolute Errors, Room type ' int2str(tip)])
s1_by=sum(abs(max_rm-max_by))/length(max_rm)

disp(['Fill Percent, Room type ' int2str(tip)])
s2_by=length(find(max_by>1))/length(max_rm)*100
% DISPLAY THE SUCCESS MEASURES

=====
=====

```

```

function voron_map(type)
% VORONOI DIAGRAM TRACING TYPE MOTION-PLANNING BASED
% MAP BUILDING SCRIPT, UTILIZING MF, VT, ATM & DM
% GETS THE PARAMETER type TO INDICATE ROOM TYPE
% ALMOST SAME AS wall_foll_map.m, HENCE NOT FULLY COMMENTED

disp('=====')
disp(['Voronoi Tracing, Room Type ' int2str(type)])
disp('=====')

room=draw_room4(type);
[Y,X]=size(room);
print('-deps',strcat('room_def_type_',int2str(type)))

load(strcat('voron_type_',int2str(type)));

% MORPHOLOGICAL PROCESSING
x_array1=vr(1,1);
y_array1=vr(2,1);
b_array1=vr(3,1);

x_array=fix(x_array1);
y_array=fix(y_array1);
b_array=fix(b_array1);
totalsonarno=length(x_array)
base_dm=zeros(Y+500,X+500);
for son=1:length(x_array)
base_dm=sonarPut5(x_array(son),y_array(son),b_array(son),room,base_dm);
end
base=base_dm;
tic
base2=logical(sign(base));
base3=bwmorph(base2,'thin',4);

time_morph=toc

figure
colormap(gray(2))
image(2-2*base2)
grid on
xlabel('pixels','FontSize',14)
ylabel('pixels','FontSize',14)
axis equal
print('-deps',strcat('mpl_vor_type_',int2str(type)))

figure
colormap(gray(2))
image(2-2*base3)
grid on
xlabel('pixels','FontSize',14)
ylabel('pixels','FontSize',14)
axis equal

```

```

print('-deps',strcat('mp2_vor_type_',int2str(type)))

% VOTING AND THRESHOLDING
tic

thres=4;
base4=sign(floor(base/thres));
time_vote=toc

figure
colormap(gray(255))
scale=255/max(max(base));
image(255-scale*base4)
axis equal
grid on
xlabel('pixels','FontSize',14)
ylabel('pixels','FontSize',14)
print('-deps',strcat('vt1_vor_type_',int2str(type)))

figure
colormap(gray(255))
image(255-255*base4)
grid on
xlabel('pixels','FontSize',14)
ylabel('pixels','FontSize',14)
axis equal
print('-deps',strcat('vt2_vor_type_',int2str(type)))

% ATM
arcs=0;
tim_atm=0;
for son=1:length(x_array)
arcs=sonarATM2(x_array(son),y_array(son),b_array(son),room,arcs,son,tim_atm);
end

tic

[arcNo,abc,acb]=size(arcs);
arcLength=length(arcs(1,:));

for arc=1:arcNo
il=1;
if (arcs(arc,1,1)~=0) || (arcs(arc,1,2)~=0)

for pix=1:arcLength
if (arcs(arc,pix,1)~=0) || (arcs(arc,pix,2)~=0)
xx=arcs(arc,pix,1);
yy=arcs(arc,pix,2);
for scl=1:arcNo
for sc2=1:arcLength
if (arcs(scl,sc2,1)==xx) && (arcs(scl,sc2,2)==yy)

```



```

if abs(thet)<=omega/2
    E_a=1-(2*thet/omega)^2;
else
    E_a=0;
end

if sig <= (R-epsi)
    E_r=1-((sig)/(R-epsi))^2;
else
    E_r=0;
end

if abs(R-sig)<=epsi
    O_r=1-((sig-R)/epsi)^2;
else
    O_r=0;
end

p_E=E_r*E_a;
p_O=O_r*E_a;

empty_array(y+250,x+250)=empty_array(y+250,x+250)+p_E*empty_array(y+250, x
+250)*p_E;
occupied_array(y+250,x+250)=occupied_array(y+250,x+250)+p_O*occupied_array(x
(y+250,x+250)*p_O;

end
end
end
time_bayes=toc

figure
colormap(gray(255))
image(255-255*empty_array)
axis equal
grid on
xlabel('pixels','FontSize',14)
ylabel('pixels','FontSize',14)
print('-deps',strcat('bayes_e_vor_type_',int2str(type)))

figure
colormap(gray(255))
image(255-255*occupied_array)
axis equal
grid on
xlabel('pixels','FontSize',14)
ylabel('pixels','FontSize',14)
print('-deps',strcat('bayes_vor_type_',int2str(type)))

by_rm=occupied_array(251:460,251:610);
tip=type;

```

```

rm=room;
switch tip
case {1}
    alt_rm=rm(151:210,3:357);
    alt_by=by_rm(151:210,3:357);

    ust_rm=rm(1:60,3:357);
    ust_by=by_rm(1:60,3:357);

    sol_rm=rm(3:207,1:60);
    sol_by=by_rm(3:207,1:60);

    sag_rm=rm(33:207,301:360);
    sag_by=by_rm(33:207,301:360);

case {2}
    alt_rm=rm(151:210,3:357);
    alt_by=by_rm(151:210,3:357);

    ust_rm=rm(1:60,3:357);
    ust_by=by_rm(1:60,3:357);

    sol_rm=rm(3:207,1:60);
    sol_by=by_rm(3:207,1:60);

    sag_rm=rm(33:207,301:360);
    sag_by=by_rm(33:207,301:360);

case {3}
    alt_rm=rm(151:210,3:357);
    alt_by=by_rm(151:210,3:357);

    ust_rm=rm(1:60,3:357);
    ust_by=by_rm(1:60,3:357);

    sol_rm=rm(3:157,1:60);
    sol_by=by_rm(3:157,1:60);

    sag_rm=rm(53:207,301:360);
    sag_by=by_rm(53:207,301:360);

end

rml=[sag_rm' sol_rm' ust_rm alt_rm];
byl=[sag_by' sol_by' ust_by alt_by];

[Y,max_rm]=max(rml);
[Y,max_by]=max(byl);

```

```

disp(['Mean Absolute Errors, Room type ' int2str(tip)])
s1_by=sum(abs(max_rm-max_by))/length(max_rm)

disp(['Fill Percent, Room type ' int2str(tip)])
s2_by=length(find(max_by>1))/length(max_rm)*100

%=====
function base=sonarPut5(x_son,y_son,b_son,room,base)
% PLACES A TRANSDUCER PAIR AT COORDINATES (x_son,y_son) BEARING b_son INTO
% A TRUE ROOM room AND DRAWS ARCS TO THE ARRAY base
% CALLED FROM NP, VT, ATM and DM IMPLEMENTATIONS

base2=zeros(size(base));
% ALLOCATE EMPTY ARC MAP FOR PROCESSING

[Y,X]=size(room);
theta0=12.5;
the0=theta0*pi/180;
be_son=b_son*pi/180;
% GET THE SIZE OF THE ROOM, DEFINE HALF-BEAMWIDTH ANGLE AND CONVERT RADIAN
% ANGLES TO DEGREES

pa_dist=9;
% DEFINE CENTER-TO-CENTER SEPARATION OF PAIR

ang0=be_son-the0;
ang1=be_son+the0;
% GET BEAMWIDTH BOUNDARIES

x_son1=x_son-fix(pa_dist/2*sin(be_son));
x_son2=x_son+fix(pa_dist/2*sin(be_son));
y_son1=y_son-fix(pa_dist/2*cos(be_son));
y_son2=y_son+fix(pa_dist/2*cos(be_son));
% CALCULATE TRANSDUCER POSITIONS

rDist=0;
mDist=0;
k=1;
s1_ind=1;
scan_deg=0.01/pi*180;
for scan=ang0:scan_deg:ang1
    [xs,ys]=p_line2(room,x_son1,y_son1,scan,[.99,.99,.99]);
    son1scan(s1_ind,1)=xs;
    son1scan(s1_ind,2)=ys;
    s1_ind=s1_ind+1;
    if isPerp2(room,xs,ys,scan)==1

        rDist(k,1)=sqrt((xs-x_son1)^2+(ys-y_son1)^2)*1e-2;
        rDist(k,2:3)=[xs,ys];

```

```

        rDist(k,4)=scan;

        mDist(k)=pulser(rDist(k,1),0);
        k=k+1;
    end
end
dist=min(mDist);
% GET r_aa

if dist~=0;
    x_a=0;
    y_a=0;
    for scan2=ang0:1e-3:ang1
        xdraw=median([X+250, fix(250+x_son1+(dist*100*cos(-scan2))), 1]);
        ydraw=median([Y+250, fix(250+y_son1+(dist*100*sin(-scan2))), 1]);
        if (xdraw==x_a) || (ydraw==y_a)
            base2(ydraw,xdraw)=base2(ydraw,xdraw)+1;
            x_a=xdraw;
            y_a=ydraw;
        end
    end
end
% IF r_aa IS NOT ZERO, DRAW THE ARC

rDist=0;
mDist=0;
k=1;
for son2scan=1:length(son1scan)
    x_scan1=son1scan(son2scan,1);
    y_scan1=son1scan(son2scan,2);
    if doesSee(x_scan1,y_scan1,x_son1,y_son1,x_son2,y_son2,room)==1;
        rDist(k,1)=(sqrt((x_scan1-x_son1)^2+(y_scan1-y_son1)^2)+sqrt((x_scan1-x_son2)^
^2+(y_scan1-y_son2)^2))*1e-2;
        mDist(k)=pulser(rDist(k,1),0);
        k=k+1;
    end
end
dist=min(mDist);
% GET r_ab

if dist>0.09;
    b=sqrt((dist/2)^2-(pa_dist/2*1e-2)^2);
    a=dist/2;
    x_a=0;
    y_a=0;
    for scan2=be_son-pi/9:1e-3:be_son+pi/9
        xdraw=median([X+250, fix(250+(x_son1+x_son2)/2+(a*100*cos(-scan2))), 1]);
        ydraw=median([Y+250, fix(250+(y_son1+y_son2)/2+(b*100*sin(-scan2))), 1]);
        if (xdraw==x_a) || (ydraw==y_a)
            base2(ydraw,xdraw)=base2(ydraw,xdraw)+1;

```

```

        x_a=xdraw;
        y_a=ydraw;
    end
    end
    scan2=be_son-pi/9:1e-3:be_son+pi/9;
    x_sc=(x_son1+x_son2)/2+fix(a*100*cos(-scan2));
    y_sc=(y_son1+y_son2)/2+fix(b*100*sin(-scan2));
end
% IF r_ab IS LARGER THAN 9 cm (CENTER-TO-CENTER SEPARATION), DRAW THE ARC

son2scan=0;
rDist=0;
mDist=0;
k=1;
s2_ind=1;
for scan=ang0:scan_deg:angl
    [xs,ys]=p_line2(room,x_son2,y_son2,scan,[.99,.99,.99]);
    son2scan(s2_ind,1)=xs;
    son2scan(s2_ind,2)=ys;
    s2_ind=s2_ind+1;
    if isPerp2(room,xs,ys,scan)==1
        rDist(k,1)=sqrt((xs-x_son1)^2+(ys-y_son1)^2)*1e-2;
        rDist(k,2:3)=[xs,ys];
        rDist(k,4)=scan;
        mDist(k)=pulsar(rDist(k,1),0);
        k=k+1;
    end
end
dist=min(mDist);
% GET r_bb

if dist==0;
    x_a=0;
    y_a=0;
    for scan2=ang0:1e-3:angl
        xdraw=median([X+250, fix(250+x_son2+(dist*100*cos(-scan2))), 1]);
        ydraw=median([Y+250, fix(250+y_son2+(dist*100*sin(-scan2))), 1]);
        if (xdraw==x_a)||(ydraw==y_a)
            base2(ydraw,xdraw)=base2(ydraw,xdraw)+1;
            x_a=xdraw;
            y_a=ydraw;
        end
    end
end
% IF r_bb IS NOT ZERO, DRAW THE ARC

rDist=0;
mDist=0;
k=1;
for son1scan=1:length(son2scan)

```

```

        x_scan2=son2scan(son1scan,1);
        y_scan2=son2scan(son1scan,2);
        if doesSee(x_scan2,y_scan2,x_son2,y_son2,x_son1,y_son1,room)==1;
            % draw oval
            rDist(k,1)=sqrt((x_scan2-x_son2)^2+(y_scan2-y_son2)^2)+sqrt((x_scan2-x_son1)^2+(y_scan2-y_son1)^2)*1e-2;
            mDist(k)=pulsar(rDist(k,1),0);
            k=k+1;
        end
    end
    dist=min(mDist);
    % GET r_ba

    if dist>0.09;
        b=sqrt((dist/2)^2-(pa_dist/2*1e-2)^2);
        a=dist/2;

        x_a=0;
        y_a=0;
        for scan2=be_son-pi/9:1e-3:be_son+pi/9
            xdraw=median([X+250, fix(250+(x_son1+x_son2)/2+(a*100*cos(-scan2))), 1]);
            ydraw=median([Y+250, fix(250+(y_son1+y_son2)/2+(b*100*sin(-scan2))), 1]);

            if (xdraw==x_a)||(ydraw==y_a)
                base2(ydraw,xdraw)=base2(ydraw,xdraw)+1;
                x_a=xdraw;
                y_a=ydraw;
            end
        end
        scan2=be_son-pi/9:1e-3:be_son+pi/9;
        x_sc=(x_son1+x_son2)/2+fix(a*100*cos(-scan2));
        y_sc=(y_son1+y_son2)/2+fix(b*100*sin(-scan2));
    end
    % IF r_ba IS LARGER THAN 9 cm (CENTER-TO-CENTER SEPARATION), DRAW THE ARC

    base=base+base2;
    % ADD THESE ARCS TO THE GIVEN ARC MAP

    %=====
    %=====

    function [x_points,y_points,b_list,d_list]=sonarPut5_d(x_son,y_son,b_son,room,base)
    % PLACES A TRANSDUCER PAIR AT COORDINATES (x_son,y_son) BEARING b_son INTO
    % A TRUE ROOM room AND RETURNS COORDINATES AND BEARINGS OF INDIVIDUAL
    % TRANSDUCERS AS WELL AS FOUR TOF MEASUREMENTS r_aa, r_ab, r_bb, r_ba
    % CALLED FROM BAYESIAN UPDATE IMPLEMENTATIONS

    base2=zeros(size(base));
    % ALLOCATE EMPTY ARC MAP FOR PROCESSING

    [Y,X]=size(room);
    theta=12.5;

```

```

the0=theta0*pi/180;
be_son=b_son*pi/180;
% GET THE SIZE OF THE ROOM, DEFINE HALF-BEAMWIDTH ANGLE AND CONVERT RADIAN
% ANGLES TO DEGREES

pa_dist=9;
% DEFINE CENTER-TO-CENTER SEPARATION OF PAIR

ang0=be_son-the0;
ang1=be_son+the0;
% GET BEAMWIDTH BOUNDARIES

x_son1=x_son-fix(pa_dist/2*sin(be_son));
x_son2=x_son+fix(pa_dist/2*sin(be_son));
y_son1=y_son-fix(pa_dist/2*cos(be_son));
y_son2=y_son+fix(pa_dist/2*cos(be_son));
% CALCULATE TRANSDUCER POSITIONS

rDist=0;
mDist=0;
k=1;
s1_ind=1;
scan_deg=0.01/pi*180;
for scan=ang0:scan_deg:angl
    [xs,ys]=p_line2(room,x_son1,y_son1,scan,[.99,.99,.99]);
    son1scan(s1_ind,1)=xs;
    son1scan(s1_ind,2)=ys;
    s1_ind=s1_ind+1;
    if isPerp2(room,xs,ys,scan)==1
        rDist(k,1)=sqrt((xs-x_son1)^2+(ys-y_son1)^2)*1e-2;
        rDist(k,2:3)=[xs,ys];
        rDist(k,4)=scan;
        mDist(k)=pulsar(rDist(k,1),0);
        k=k+1;
    end
end
d11=min(mDist);
% CALCULATE r_aa FOR RETURN

rDist=0;
mDist=0;
k=1;
for son2scan=1:length(son1scan)
    x_scan1=son1scan(son2scan,1);
    y_scan1=son1scan(son2scan,2);
    if doesSee(x_scan1,y_scan1,x_son1,y_son1,x_son2,y_son2,room)==1;
        rDist(k,1)=sqrt((x_scan1-x_son1)^2+(y_scan1-y_son1)^2)+sqrt((x_scan1-x_son2)^2+(y_scan1-y_son2)^2)*1e-2;
        mDist(k)=pulsar(rDist(k,1),0);
        k=k+1;
    end
end

```

```

end
dist=min(mDist);
if dist>0.09
    d22=sqrt((dist/2)^2-(pa_dist/2*1e-2)^2);
else
    d22=0;
end
% CALCULATE r_ab FOR RETURN

son2scan=0;
rDist=0;
mDist=0;
k=1;
s2_ind=1;
for scan=ang0:scan_deg:angl
    [xs,ys]=p_line2(room,x_son2,y_son2,scan,[.99,.99,.99]);
    son2scan(s2_ind,1)=xs;
    son2scan(s2_ind,2)=ys;
    s2_ind=s2_ind+1;
    if isPerp2(room,xs,ys,scan)==1

        rDist(k,1)=sqrt((xs-x_son1)^2+(ys-y_son1)^2)*1e-2;
        rDist(k,2:3)=[xs,ys];
        rDist(k,4)=scan;

        mDist(k)=pulsar(rDist(k,1),0);
        k=k+1;
    end
end
d33=min(mDist);
% CALCULATE r_bb FOR RETURN

rDist=0;
mDist=0;
k=1;
for son1scan=1:length(son2scan)
    x_scan2=son2scan(son1scan,1);
    y_scan2=son2scan(son1scan,2);
    if doesSee(x_scan2,y_scan2,x_son2,y_son2,x_son1,y_son1,room)==1;
        rDist(k,1)=sqrt((x_scan2-x_son2)^2+(y_scan2-y_son2)^2)+sqrt((x_scan2-x_son1)^2+(y_scan2-y_son1)^2)*1e-2;
        mDist(k)=pulsar(rDist(k,1),0);
        k=k+1;
    end
end
dist=min(mDist);
if dist>0.09
    d44=sqrt((dist/2)^2-(pa_dist/2*1e-2)^2);
else

```

```

d44=0;
end
% CALCULATE r_ba FOR RETURN

x_points=[x_son1,x_son,x_son2,x_son];
y_points=[y_son1,y_son,y_son2,y_son];
b_list=[b_son,b_son,b_son,b_son];
d_list=[d11,d22,d33,d44];
% COMBINE LOACTIONS, BEARINGS AND MEASUREMENTS

%=====
%=====

function measured=pulser(dist,drawWave)
% USING THE SIGNAL MODEL, SIMULATES THE ECHO AND PERFORMS SIMPLE
% THRESHOLDING. RETURNS THE RANGE FOR THE ESTIMATED TOF FOR GIVEN DISTANCE dist
% CALLED FROM sonar_Put5.m AND sonar_Put5_d.m

f0=49.4e3;
tao=2e-9;
c=343.3;
t_trip=2*dist/c;
t_d=1.1e-4;
thresh=2.75*1e-2;
r_min=0.057;
k=35;
% DEFINE THE PARAMETERS

for k=1:2.2e2;
    t(k)=k*1e-6;
    pulse(k)=k*(r_min/dist)*sin(2*pi*f0*(t(k)-t_d))*exp(-(t(k)-t_d)^2/tao);
end
% FORM THE GAUSSIAN MODULATED SINUSOID

p1=zeros(1,4.7e4);
offset_trip=fix(t_trip/1e-6);
p1(offset_trip+1:offset_trip+length(pulse))=pulse;
% SHIFT THE SINUSOID TO ACTUAL TOF

p1=p1+5e-3*randn(1,length(p1));
% APPLY THE ZERO MEAN GAUSSIAN NOISE

tim=linspace(0,4.7e4*1e-6,length(p1));
if drawWave==1
    figure
    plot(tim,p1)
    hold on
    plot(tim,thresh*ones(1,length(p1)),'r')
    xlabel('time')
    ylabel('amplitude')
    legend('signal','threshold')
    grid on
end

```

```

son2ang=atan2(y2-ys,xs-x2);
normAng=(son2ang+sonlang)/2;

sees=0;
tol=7;
ang2=normAng+pi/2;
x_c1=median([1,xs+fix(tol*cos(ang2)),X]);
x_c2=median([1,xs-fix(tol*cos(ang2)),X]);
y_c1=median([1,ys+fix(tol*sin(ang2)),Y]);
y_c2=median([1,ys-fix(tol*sin(ang2)),Y]);

if rm(y_c1,x_c1)~=0
    if rm(y_c2,x_c2)~=0
        sees=1;
    end
end

%=====
%=====

function room=draw_room4(type)
% DRAWS AND RETURN THE ROOM TYPE type

X=360;
Y=210;
room=zeros(Y,X);
room(1:3,1:180)=ones(3,180);
room(28:30,181:360)=ones(3,180);
room(1:30,178:180)=ones(30,3);
room(1:210,1:3)=ones(210,3);
room(30:210,358:360)=ones(181,3);
room(208:210,1:360)=ones(3,360);

switch type
case {1}

case {2}
    room(208:210,110:250)=zeros(3,141);
    room(158:160,108:250)=ones(3,143);
    room(160:210,108:110)=ones(51,3);
    room(160:210,248:250)=ones(51,3);

case {3}
    room(28:30,181:360)=zeros(3,180);
    room(48:50,171:360)=ones(3,190);
    room(1:30,178:180)=zeros(30,3);
    room(1:50,168:170)=ones(50,3);
    room(1:3,171:180)=zeros(3,10);
    room(208:210,1:180)=zeros(3,180);
    room(158:160,1:180)=ones(3,180);
    room(160:210,178:180)=ones(51,3);
    room(161:210,1:3)=zeros(50,3);
end

```

```

end
% DISPLAY THE SIGNAL

measured=0;
found=0;
for k=1:length(p1)
    if p1(k)>thresh
        if found==0;
            measured=k;
            found=1;
        end
    end
end
% CALCULATE THE TOF

measured=measured*1e-6/2*343.3;
% RETURN THE RANGE

%=====
%=====

function perp=isPerp2(room,x_son,y_son,ang1)
% CHECKS IF THE RAY FROM POSITION x_son, y_son BEARING b_son HAS
% PERPENDICULAR INCIDENCE ON ANY SURFACE IN ENVIRONMENT room
% CALLED FROM TRANSDUCER PLACEMENT FUNCTIONS

[Y,X]=size(room);
perp=0;
tol=10;
ang2=ang1+pi/2;
x_c1=median([1,x_son+fix(tol*cos(ang2)),X]);
x_c2=median([1,x_son-fix(tol*cos(ang2)),X]);
y_c1=median([1,y_son+fix(tol*sin(ang2)),Y]);
y_c2=median([1,y_son-fix(tol*sin(ang2)),Y]);

if room(y_c1,x_c1)~=0
    if room(y_c2,x_c2)~=0
        perp=1;
    end
end

%=====
%=====

function sees=doesSee(xs,ys,x1,y1,x2,y2,rm)
% CHECKS OF THE RAY FROM TRANSDUCER A AT (x1,y1) REFLECTS FROM POINT (xs,ys) IN rm TO
% TRANSDUCER B AT (x2,y2)

[Y,X]=size(rm);

sonlang=atan2(y1-ys,xs-x1);

```

```

room(1:48,358:360)=zeros(48,3);

end

figure
colormap(gray(255))
image(255-255*(room))
axis equal
grid on;
xlabel('pixels','FontSize',14)
ylabel('pixels','FontSize',14)
% DISPLAY THE ROOM

%=====
%=====

function wall_foll2(type)
% CREATES WALL FOLLOWING STEPS IN ROOM TYPE type

clc
tic
room=draw_room4(type);
% DRAW THE ROOM
[Y,X]=size(room);
% GET THE SIZE
base=zeros(Y+500,X+500);
% ALLOCATE THE EMPTY ARRAY FOR MEASUREMENTS
sal=0;
initialX=60;
initialY=100;
initialB=0;
% SET THE INITIAL POSITIONS

text(initialX,initialY,'R')

directionN=16;
b_array=linspace(0,360-360/directionN,directionN)+initialB*ones(1,directionN);
x_array=initialX*ones(1,directionN);
y_array=initialY*ones(1,directionN);
% GET THE FIRST LOOK DIRECTIONS

for son=1:directionN
    d_array(son)=sonarPut_d(x_array(son),y_array(son),b_array(son),room,base);
end
% FIRST LOOK IN 16 DIRECTIONS

[md,ind]=min(d_array);
kk=1;
while md==0
    d_array(ind)=1000+kk;
    kk=kk+1;
    [md,ind]=min(d_array);
end

```



```

end
wall_dir=mod(b_array(ind),360)
% DECIDE ON CLOSEST WALL DIRECTION

md=md*100

x_fs=initialX+fix((md-60)*cosd(wall_dir));
y_fs=initialY-fix((md-60)*sind(wall_dir));
b_fs=wall_dir-90;
step_no=1;
text(x_fs,y_fs,'1')
x_loc(step_no)=x_fs;
y_loc(step_no)=y_fs;
b_loc(step_no)=b_fs;
step_no=step_no+1;
% FIRST STEP

while step_no<100
step_no
[d1,d2]=look1(x_fs,y_fs,b_fs,room,base)

if d2>80
b_fs=b_fs+90;
x_fs=x_fs+fix(20*cosd(b_fs));
y_fs=y_fs-fix(20*sind(b_fs));

text(x_fs,y_fs,int2str(step_no))
x_loc(step_no)=x_fs;
y_loc(step_no)=y_fs;
b_loc(step_no)=b_fs;
step_no=step_no+1;

x_fs=x_fs+fix(20*cosd(b_fs));
y_fs=y_fs-fix(20*sind(b_fs));

text(x_fs,y_fs,int2str(step_no))
x_loc(step_no)=x_fs;
y_loc(step_no)=y_fs;
b_loc(step_no)=b_fs;
step_no=step_no+1;

x_fs=x_fs+fix(24*cosd(b_fs));
y_fs=y_fs-fix(24*sind(b_fs));

text(x_fs,y_fs,int2str(step_no))
x_loc(step_no)=x_fs;
y_loc(step_no)=y_fs;
b_loc(step_no)=b_fs;
step_no=step_no+1;
else
if d1>60

```

```

switch type
case {1}
for scan=1:length(vv)
if ((vv(scan,1)>180) || (vv(scan,2)>180)) && ((vv(scan,3)<30) || (vv(scan,4)<30))
vv(scan,:)=zeros(1,4);
end
case {2}
for scan=1:length(vv)
if ((vv(scan,1)>180) || (vv(scan,2)>180)) && ((vv(scan,3)<30) || (vv(scan,4)<30)) &
|| ((vv(scan,1)<250) || (vv(scan,2)<250)) && ((vv(scan,1)>110) || (vv(scan,2)>110)) && ((vv(scan,3)
>160) || (vv(scan,4)>160))
vv(scan,:)=zeros(1,4);
end
case {3}
for scan=1:length(vv)
if ((vv(scan,1)>170) || (vv(scan,2)>170)) && ((vv(scan,3)<50) || (vv(scan,4)<50)) &
|| ((vv(scan,1)<180) || (vv(scan,2)<180)) && ((vv(scan,3)>160) || (vv(scan,4)>160))
vv(scan,:)=zeros(1,4);
end
end
% ELIMINATE THE EDGES PARTIALLY OUTSIDE THE ROOM

vv=vv';
vx(1,:)=vv(1,:);
vx(2,:)=vv(2,:);
vy(1,:)=vv(3,:);
vy(2,:)=vv(4,:);

figure
plot(x_array,y_array,'r.',vx,vy,'b');
axis equal
grid on
xlabel('pixels','FontSize',14)
ylabel('pixels','FontSize',14)
print('-deps',strcat('voron_diagram_type_',int2str(type)))
z(1,:)=vv(1,:);
z(2,:)=vv(3,:);
z2(1,:)=vv(2,:);
z2(2,:)=vv(4,:);
z3=[z z2];
z4=unique(z3,'rows');
% DISPLAY AND EXPORT THE FULL VORONOI DIAGRAM WITH THE ROOM

figure
plot(z4(:,1),z4(:,2),'.')
grid on
xlabel('pixels','FontSize',14)
ylabel('pixels','FontSize',14)
print('-deps',strcat('voron_diagram_allpoints_type_',int2str(type)))

```

```

x_fs=x_fs+fix(14*cosd(b_fs));
y_fs=y_fs-fix(14*sind(b_fs));

x_fs=x_fs+fix((d2-60)*cosd(b_fs+90));
y_fs=y_fs-fix((d2-60)*sind(b_fs+90));

text(x_fs,y_fs,int2str(step_no))
x_loc(step_no)=x_fs;
y_loc(step_no)=y_fs;
b_loc(step_no)=b_fs;
step_no=step_no+1;
else
b_fs=b_fs-90;
end
end
if (abs(x_fs-initialX)<20) && (abs(y_fs-initialY)<20) && (step_no>10)
break
end
end
% TILL THE END OF STEPS, ACCORDING TO THE DECISION RULES

wf=[x_loc; y_loc; b_loc];
save(strcat('wall_foll_type_',int2str(type)),'wf')
print('-deps',strcat('wf_steps_type_',int2str(type)))
% SAVE AND DISPLAY THE STEP POSITIONS

%=====
%=====

function voron2(type)
% CREATES VORONOI DIAGRAM OF THE ROOM type AND SAMPLE POINTS

room=draw_room3(type);
% DEFINE THE ROOM

[Y,X]=size(room);
ind=1;
for x=1:X
for y=1:Y
if room(y,x)==1;
y_array(ind)=y;
x_array(ind)=x;
ind=ind+1;
end
end
end
% GET THE FULL PIXEL LOCATIONS

[vx,vy]=voronoi(x_array,y_array);
vv=[vx' vy'];
% CREATE THE VORONOI DIAGRAM

```

```

% DISPLAY AND EXPORT VORONOI DIAGRAM ALL POINTS WITHOUT THE ROOM

rr=3;
for samp=1:floor(length(z4)/rr)
z42(samp,:)=z4(samp*rr,:);
end;
zscan2=1;
for zscan=1:length(z42)
xx=z42(zscan,1);
yy=z42(zscan,2);
switch type
case {1}
if ((xx<20) && (yy<20 || yy>190)) || ((xx<180) && (xx>160) && (yy<20)) || ((xx>340) &
&& (yy<50) || (yy>190))
z42(zscan,:)=zeros(1,2);
end
case {2}
if ((xx<20) && (yy<20 || yy>190)) || ((xx<180) && (xx>150) && (yy<20)) || ((xx>340) &
&& (yy<50) || (yy>190)) || ((xx<110) && (xx>90) && (yy>190)) || ((xx>250) && (xx<270) && (yy>190))
z42(zscan,:)=zeros(1,2);
end
case {3}
if ((xx<20) && (yy<20 || yy>140)) || ((xx<180) && (xx>150) && (yy<20)) || ((xx>340) &
&& (yy<70) || (yy>190)) || ((xx<200) && (xx>170) && (yy>190))
z42(zscan,:)=zeros(1,2);
end
end
if z42(zscan,1)~=0
z43(zscan2,:)=z42(zscan,:);
zscan2=zscan2+1;
end
end
% SAMPLE THE VORONOI DIAGRAM POINTS AND ELIMINATE THE ONES TOO CLOSE TO
% CORNERS

z42=z43;
room=draw_room4(type);
hold on
plot(z42(:,1),z42(:,2),'.')
grid on
xlabel('pixels','FontSize',14)
ylabel('pixels','FontSize',14)
print('-deps',strcat('voron_diagram_samples_type_',int2str(type)))
clear x_array y_array
z42=fix(z42);
% z42=fix(z42);
base=0;
direc=[0,90,180,270];
% DISPLAY AND EXPORT THE VORONOI DIAGRAM SAMPLES

```

```

array_in=1;
for tara=1:length(z42)
    for yon=1:4
        direc_d(yon)=sonarPut_d(z42(tara,1),z42(tara,2),direc(yon),room,base);
    end
    dl=min(direc_d);
    dirs=find(abs(direc_d-dl)<0.1);
    for ek=1:length(dirs)
        x_array(array_in)=z42(tara,1);
        y_array(array_in)=z42(tara,2);
        b_array(array_in)=direc(dirs(ek));
        array_in=array_in+1;
    end
end
% CALCULATE THE MEASUREMENT DIRECTIONS FROM SAMPLE POINTS

vr=[x_array; y_array; b_array];
save(strcat('voronoi_type_',int2str(type)),'vr')
% SAVE THE VORONOI DIAGRAM TRACING MEASUREMENT POSITIONS AND BEARINGS

%=====
%=====

function [mean_err,fill_per]=room_suc(tip,rm,mp_room,vt_room,atm_room,dm_room)
% CALCULATES AND DISPLAY SUCCESS MEASURES MEAN ABSOLUTE ERROR AND FILL
% PERCENT FOR MP, VT, ATM AND DM

mp_rm=mp_room(251:460,251:610);
vt_rm=vt_room(251:460,251:610);
atm_rm=atm_room(251:460,251:610);
dm_rm=dm_room(251:460,251:610);
mean_err=0;
fill_per=0;

switch tip
case {1}
    alt_rm=rm(151:210,3:357);
    alt_mp=mp_rm(151:210,3:357);
    alt_vt=vt_rm(151:210,3:357);
    alt_atm=atm_rm(151:210,3:357);
    alt_dm=dm_rm(151:210,3:357);

    ust_rm=rm(1:60,3:357);
    ust_mp=mp_rm(1:60,3:357);
    ust_vt=vt_rm(1:60,3:357);
    ust_atm=atm_rm(1:60,3:357);
    ust_dm=dm_rm(1:60,3:357);

    sol_rm=rm(3:207,1:60);
    sol_mp=mp_rm(3:207,1:60);
    sol_vt=vt_rm(3:207,1:60);
    sol_atm=atm_rm(3:207,1:60);
end

```

```

    sol_dm=dm_rm(3:207,1:60);

    sag_rm=rm(33:207,301:360);
    sag_mp=mp_rm(33:207,301:360);
    sag_vt=vt_rm(33:207,301:360);
    sag_atm=atm_rm(33:207,301:360);
    sag_dm=dm_rm(33:207,301:360);
case {2}
    alt_rm=rm(151:210,3:357);
    alt_mp=mp_rm(151:210,3:357);
    alt_vt=vt_rm(151:210,3:357);
    alt_atm=atm_rm(151:210,3:357);
    alt_dm=dm_rm(151:210,3:357);

    ust_rm=rm(1:60,3:357);
    ust_mp=mp_rm(1:60,3:357);
    ust_vt=vt_rm(1:60,3:357);
    ust_atm=atm_rm(1:60,3:357);
    ust_dm=dm_rm(1:60,3:357);

    sol_rm=rm(3:207,1:60);
    sol_mp=mp_rm(3:207,1:60);
    sol_vt=vt_rm(3:207,1:60);
    sol_atm=atm_rm(3:207,1:60);
    sol_dm=dm_rm(3:207,1:60);

    sag_rm=rm(33:207,301:360);
    sag_mp=mp_rm(33:207,301:360);
    sag_vt=vt_rm(33:207,301:360);
    sag_atm=atm_rm(33:207,301:360);
    sag_dm=dm_rm(33:207,301:360);
case {3}
    alt_rm=rm(151:210,3:357);
    alt_mp=mp_rm(151:210,3:357);
    alt_vt=vt_rm(151:210,3:357);
    alt_atm=atm_rm(151:210,3:357);
    alt_dm=dm_rm(151:210,3:357);

    ust_rm=rm(1:60,3:357);
    ust_mp=mp_rm(1:60,3:357);
    ust_vt=vt_rm(1:60,3:357);
    ust_atm=atm_rm(1:60,3:357);
    ust_dm=dm_rm(1:60,3:357);

    sol_rm=rm(3:157,1:60);
    sol_mp=mp_rm(3:157,1:60);
    sol_vt=vt_rm(3:157,1:60);
    sol_atm=atm_rm(3:157,1:60);
    sol_dm=dm_rm(3:157,1:60);

    sag_rm=rm(53:207,301:360);
    sag_mp=mp_rm(53:207,301:360);
end

```

```

    sag_vt=vt_rm(53:207,301:360);
    sag_atm=atm_rm(53:207,301:360);
    sag_dm=dm_rm(53:207,301:360);
end

rml=[sag_rm' sol_rm' ust_rm alt_rm];
mpl=[sag_mp' sol_mp' ust_mp alt_mp];
vtl=[sag_vt' sol_vt' ust_vt alt_vt];
atml=[sag_atm' sol_atm' ust_atm alt_atm];
dml=[sag_dm' sol_dm' ust_dm alt_dm];
% RESHAPE THE GIVEN ARC MAP AND TRUE ROOM FOR COMPARISON

[Y,max_rm]=max(rml);
[Y,max_mp]=max(mpl);
[Y,max_vt]=max(vtl);
[Y,max_atm]=max(atml);
[Y,max_dm]=max(dml);

disp(['Mean Absolute Errors, Room type ' int2str(tip)])
s1_mp=sum(abs(max_rm-max_mp))/length(max_rm)
s1_vt=sum(abs(max_rm-max_vt))/length(max_rm)
s1_atm=sum(abs(max_rm-max_atm))/length(max_rm)
s1_dm=sum(abs(max_rm-max_dm))/length(max_rm)

disp(['Fill Percent, Room type ' int2str(tip)])
s2_mp=length(find(max_mp>1))/length(max_rm)*100
s2_vt=length(find(max_vt>1))/length(max_rm)*100
s2_atm=length(find(max_atm>1))/length(max_rm)*100
s2_dm=length(find(max_dm>1))/length(max_rm)*100

mean_err=[s1_mp s1_vt s1_atm s1_dm];
fill_per=[s2_mp s2_vt s2_atm s2_dm];
% CALCULATE AND RETURN THE SUCCESS MEASURES

```

# Bibliography

- [1] B. Ayrulu and B. Barshan. Identification of target primitives with multiple decision-making sonars using evidential reasoning. *International Journal of Robotics Research*, 17(6):598–623, June 1998.
- [2] J. L. Crowley. Navigation for an intelligent mobile robot. *IEEE Transactions on Robotics and Automation*, RA-1(1):31–41, March 1985.
- [3] A. Elfes. Sonar based real-world mapping and navigation. *IEEE Transactions on Robotics and Automation*, RA-3(3):249–265, June 1987.
- [4] A. Elfes. Using occupancy grids for mobile robot perception and navigation. *IEEE Computer*, 22(6):46–57, 1989.
- [5] H. F. Durrant-Whyte and I. J. Cox. Dynamic map building for an autonomous mobile robot. In *Proceedings IEEE/RSJ International Workshop on Intelligent Robots and Systems*, pages 89–96, Tsuchiura, Ibaraki, Japan, 3–6 July 1990.
- [6] D. Maksarov and H. F. Durrant-Whyte. Mobile vehicle navigation in unknown environments—a multiple hypothesis approach. *IEE Proceedings—Control Theory and Applications*, 142(4):385–400, July 1995.
- [7] A. Kurz. Constructing maps for mobile robot navigation based on ultrasonic range data. *IEEE Transactions on Systems, Man, and Cybernetics—Part B: Cybernetics*, 26(2):233–242, April 1996.
- [8] M. Kulich, P. Stepan, and L. Preucil. Feature detection and map building using ranging sensors. In *Proceedings of the IEEE International Conference on*

- Intelligent Transportation*, volume 1, pages 201–206, Tokyo, Japan, October 1999.
- [9] T. Bailey, E. M. Nebot, J. K. Rosenblatt, and H. F. Durrant-Whyte. Data association for mobile robot navigation: a graph theoretic approach. In *Proceedings of IEEE International Conference on Robotics and Automation*, volume 3, pages 2512–2517, San Francisco, CA, U.S.A., 24–27 April 2000.
- [10] R. Kuc and M. W. Siegel. Physically-based simulation model for acoustic sensor robot navigation. *IEEE Transactions on Pattern Analysis and Machine Intelligence*, PAMI-9(6):766–778, November 1987.
- [11] B. Barshan and R. Kuc. Differentiating sonar reflections from corners and planes by employing an intelligent sensor. *IEEE Transactions on Pattern Analysis and Machine Intelligence*, 12(6):560–569, June 1990.
- [12] H. Peremans, K. Audenaert, and J. M. Van Campenhout. A high-resolution sensor based on tri-aural perception. *IEEE Transactions on Robotics and Automation*, 9(1):36–48, February 1993.
- [13] L. Kleeman and R. Kuc. Mobile robot sonar for target localization and classification. *International Journal of Robotics Research*, 14(4):295–318, August 1995.
- [14] M. L. Hong and L. Kleeman. Ultrasonic classification and location of 3-D room features using maximum likelihood estimation I. *Robotica*, 15(Part 5):483–491, September/October 1997.
- [15] R. Kuc. Biomimetic sonar recognizes objects using binaural information. *The Journal of the Acoustical Society of America*, 102(2):689–696, August 1997.
- [16] J. Bruce and M. Veloso. Real-time randomized path planning for robot navigation. In *Proceedings of the IEEE/RSJ International Conference on Intelligent Robots and Systems*, volume 3, pages 2383–2388, Lausanne, Switzerland, 30 September–5 October 2002.
- [17] D. Fox, W. Burgard, and S. Thrun. The dynamic window approach to collision avoidance. *IEEE Robotics and Automation Magazine*, 4(1):23–33, March 1997.

- [18] D. Hsu, R. Kindel, C. Latombe, and S. Rock. Randomized kinodynamic motion planning with moving obstacles. *International Journal of Robotics Research*, 21(3):233–255, 2002.
- [19] T. Yata, L. Kleeman, and S. Yuta. Wall following using angle information measured by a single ultrasonic transducer. In *Proceedings of IEEE International Conference on Robotics and Automation*, volume 5, pages 1590–1596, Leuven, Belgium, 16–21 May 1998.
- [20] X. Yun and K.-C. Tan. A wall-following method for escaping local minima in potential field based motion planning. In *Proceedings of the IEEE International Conference on Advanced Robotics*, pages 421–426, Monterey, CA, U.S.A., 7–9 July 1997.
- [21] A. Bemporad, M. Di Marco, and A. Tesi. Wall-following controllers for sonar-based mobile robots. In *Proceedings of the IEEE International Conference on Decision and Control*, volume 8, pages 3063–3068, San Diego, CA, U.S.A., December 1997.
- [22] D. Lee and M. Recce. Quantitative evaluation of the exploration strategies of an intelligent vehicle. *International Journal of Robotics Research*, 16(4):413–447, August 1994.
- [23] E. Tunstel and M. Jamshidi. Embedded fuzzy logic-based wall-following behavior for mobile robot navigation. In *Proceedings of 1st International Joint Conference of NAFIPS/IFIS/NASA*, pages 329–330, San Antonio, TX, U.S.A., 18–21 December 1994.
- [24] H. Choset, I. Konukseven, and J. Burdick. Mobile robot navigation: issues in implementating the generalized Voronoi graph in the plane. In *Proceedings IEEE/SICE/RSJ International Conference on Multisensor Fusion and Integration for Intelligent Systems*, pages 241–248, Washington D.C., U.S.A., 8–11 December 1996.
- [25] H. Choset and J. Burdick. Sensor-based exploration: The hierarchical generalized Voronoi graph. *International Journal of Robotics Research*, 19(2):96–125, February 2000.

- [26] H. Choset, S. Walker, K. Eiamsa-Ard, et al. Sensor-based exploration: Incremental construction of the hierarchical generalized Voronoi graph. *International Journal of Robotics Research*, 19(2):126–148, February 2000.
- [27] J. Zemanek. Beam behavior within the nearfield of a vibrating piston. *The Journal of the Acoustical Society of America*, 49(1 (Part 2)):181–191, January 1971.
- [28] B. Barshan. *A Sonar-Based Mobile Robot for Bat-Like Prey Capture*. PhD thesis, Yale University, Department of Electrical Engineering, New Haven, CT, U.S.A., December 1991.
- [29] H. R. Everett. *Sensors for Mobile Robots, Theory and Application*. A K Peters, Ltd., 289 Linden St, Wellesley, MA, 1995.
- [30] A. Papoulis. *Probability, Random Variables and Stochastic Processes*. McGraw-Hill, New York, NY, 3rd edition, 1991.
- [31] W. G. McMullan, B. A. Delanghe, and J. S. Bird. A simple rising-edge detector for time-of-arrival estimation. *IEEE Transactions on Instrumentation and Measurement*, 45(4):823–827, August 1996.
- [32] B. Barshan and R. Kuc. A bat-like sonar system for obstacle localization. *IEEE Transactions on Systems Man and Cybernetics*, 22(4):636–646, July/August 1992.
- [33] J. J. Leonard and H. F. Durrant-Whyte. *Directed Sonar Navigation*. Kluwer Academic Press, London, U.K., 1992.
- [34] D. Başkent and B. Barshan. Surface profile determination from multiple sonar data using morphological processing. *International Journal of Robotics Research*, 18(8):788–808, August 1999.
- [35] B. Barshan and D. Başkent. Morphological surface profile extraction with multiple range sensors. *Pattern Recognition*, 34(7):1459–1467, July 2001.
- [36] Polaroid Corporation, Ultrasonic Components Group, 119 Windsor St., Cambridge, MA. *Polaroid Manual*, 1997.

- [37] B. Barshan and D. Bařkent. Comparison of two methods of surface profile extraction from multiple ultrasonic range measurements. *Measurement Science and Technology*, 11(6):833–844, June 2000.
- [38] B. Barshan. Ultrasonic surface profile determination by spatial voting. *Electronics Letters*, 35(25):2232–2234, 9 December 1999.
- [39] H. Choset, K. Nagatani, and N. Lazar. The arc-transversal median algorithm: a geometric approach to increasing ultrasonic sensor azimuth accuracy. *IEEE Transactions on Robotics and Automation*, 19(3):513–522, June 2003.
- [40] H. P. Moravec and A. Elfes. High resolution maps from wide angle sonar. In *Proceedings of IEEE International Conference on Robotics and Automation*, pages 116–121, San Francisco, CA, U.S.A., 7–10 April 1986.
- [41] H. Moravec. Sensor fusion in certainty grids for mobile robots. *AI Magazine*, Summer:61–74, 1988.
- [42] J. Serra. *Image Analysis and Mathematical Morphology*. Academic Press, New York, NY, 1982.
- [43] Y. D. Chen and E. R. Dougherty. Gray-scale morphological granulometric texture classification. *Optical Engineering*, 33(8):2713–2722, August 1994.
- [44] J. G. Verly and R. L. Delanoy. Some principles and applications of adaptive mathematical morphology for range imagery. *Optical Engineering*, 32(12):3295–3306, December 1993.
- [45] A. Mojsilovic, M. Popovic, N. Amodaj, R. Babic, and M. Ostojic. Automatic segmentation of intravascular ultrasound images: A texture-based approach. *Annals of Biomedical Engineering*, 25(6):1059–1071, November/December 1997.
- [46] M. B. Holder, M. M. Trivedi, and S. B. Marapane. Mobile robot navigation by wall following using a rotating ultrasonic scanner. In *Proceedings of the 13th International Conference on Pattern Recognition*, volume 3, pages 298–302, 25–29 August 1996.